

Symmetry Breaking and the Generation of Spin Ordered Magnetic States in Density Functional Theory due to Dirac Exchange for a Hydrogen Molecule

Michael Holst^{*} Houdong Hu[†] Jianfeng Lu[‡] Jeremy L. Marzuola[§] Duo Song[¶]
 John Weare^{||}

February 24, 2021

Abstract

We study symmetry breaking in the mean field solutions to the electronic structure problem for the 2 electron hydrogen molecule within the Kohn Sham (KS) local spin density functional theory with Dirac exchange (the XLDA model). This simplified model shows behavior related to that of the (KS) spin density functional theory (SDFT) predictions in condensed matter and molecular systems. The KS solutions to the constrained SDFT variation problem undergo spontaneous symmetry breaking leading to the formation of spin ordered states as the relative strength of the non-convex exchange term increases. Numerically, we observe that with increases in the internuclear bond length the molecular ground state changes from a paramagnetic state (spin delocalized) to an antiferromagnetic (spin localized) ground state and a symmetric delocalized (spin delocalized) excited state. We further characterize the limiting behavior of the minimizer when the strength of the exchange term goes to infinity both analytically and numerically. This leads to further bifurcations and highly localized states with varying character. Finite element numerical results provide support for the formal conjectures. Various solution classes are found to be numerically stable. However, for changes in the R parameter, numerical Hessian calculations demonstrate that these are stationary but not stable solutions.

1 Introduction

In this paper, we report studies of the properties of density functional theory (DFT) energy minimizers within the context of the hydrogen molecule, H_2 . The (DFT) minimizers discussed are related to those of the Kohn-Sham spin density functional method. The exchange correlation function [50] is simplified

^{*}Department of Mathematics, University of California, San Diego, 9500 Gilman Dr. La Jolla, CA 92093, USA (mholst@math.ucsd.edu).

[†]Microsoft Corporation, Bellevue, WA, USA (vincehouhou@gmail.com).

[‡]Department of Mathematics, Department of Physics, and Department of Chemistry, Duke University, Box 90320, Durham, NC 27708, USA (jianfeng@math.duke.edu).

[§]Department of Mathematics, University of North Carolina at Chapel Hill, CB#3250 Phillips Hall, Chapel Hill, NC 27599, USA (marzuola@math.unc.edu).

[¶]Physical and Computational Sciences Directorate, Pacific Northwest National Laboratory, Richland, WA 99354, USA (duo.song@pnl.gov).

^{||}Department of Chemistry, University of California, San Diego, 9500 Gilman Dr., La Jolla, CA 92093, USA (jweare@ucsd.edu).

by including only Dirac spin density exchange without correlation [50]. We will show that for fixed electron mass, the structure of the minimizing Kohn-Sham solutions change character with the variation of parameters related to the relative strength of the exchange-correlation component of the functional. In particular, the changes of these parameters lead to bifurcations from globally stable delocalized product states with no spin localization to product states with electron spin localized on atomic sites (antiferromagnetic states). This behavior is similar to the formation of spin ordered states in the DFT analysis of highly correlated materials [18, 22, 51, 56].

Similar studies varying the molecular bond length have been undertaken using robust finite element methods for Hartree-Fock and SLDA functionals in [35] and for Hartree-Fock using a maximum overlap method in [7]. The precise electron configurations that occur in the ground states of such problems is important for further developing density functional theory (see e.g., [19, 20]) as well as directly in the application of density functional theory (DFT) to highly correlated condensed materials [18, 22, 51, 56] and in spin ordered molecular systems. In addition, uniqueness and symmetry breaking in other quantum mechanical models have recently been studied widely in for instance the works [25, 26] for polaron models, [29, 30, 31] for Hartree-Fock models of atoms, and many others. A similar strategy to that undertaken here in one of our limits was explored for the periodic Thomas–Fermi–Dirac–von Weizsäcker model in [54, 55].

We consider a neutral hydrogen molecule H_2 with nuclei placed $2R$ apart. The external potential is given by (after a possible coordinate change)

$$V_R(x) = -\frac{1}{|x - Re_1|} - \frac{1}{|x + Re_1|}, \quad (1)$$

where e_1 is the $(1, 0, 0)$ vector in \mathbb{R}^3 . The two-electron Schrödinger operator is given by

$$H_2 = -\frac{1}{2}\Delta_{x_1} - \frac{1}{2}\Delta_{x_2} + V_R(x_1) + V_R(x_2) + \frac{1}{|x_1 - x_2|}, \quad (2)$$

where x_1 and x_2 denote the position of the two electrons in the system. Atomic units are used throughout.

In this work, we will consider the spin-polarized density functional theory with the exchange energy taken to be Dirac exchange and without correlation energy. In the literature, the spin free version of this model is sometimes referred as the XLDA model. We are interested in the spin paired ground state of the system with spin up ψ_+ and spin down ψ_- spatial wave functions. We would like to study the impact of the exchange term on the electronic structure. Therefore, we introduce a strength parameter $\alpha \geq 0$ for the exchange energy functional. The DFT energy functional is hence given by

$$\begin{aligned} \mathcal{E}_\alpha(\psi_+, \psi_-) = & \frac{1}{2} \int |\nabla \psi_+|^2 dx + \frac{1}{2} \int |\nabla \psi_-|^2 dx + \int V_R(x) \rho(x) dx \\ & + \frac{1}{2} \iint \frac{\rho(x)\rho(y)}{|x-y|} dx dy - \alpha \int (|\psi_+|^{8/3} + |\psi_-|^{8/3}) dx, \end{aligned} \quad (3)$$

where the electron density of the system is given by

$$\rho(x) = |\psi_+(x)|^2 + |\psi_-(x)|^2. \quad (4)$$

Note in particular in (3) the Dirac exchange term is spin-polarized: let $\rho_\pm = |\psi_\pm|^2$ be the spin-polarized densities, the exchange term is given by

$$- \alpha \int (\rho_+^{4/3} + \rho_-^{4/3}) dx \quad (5)$$

as the exchange effect originating from Pauli's exclusion principle only occurs between electrons with same spin polarization [48, 50].

The potential V_R defined in (1) corresponds to the H_2 molecule having reflection symmetry. We are interested in the symmetry (delocalization) (or lack of symmetry, localization) of ψ_+ and ψ_- . In particular, when a solution inherits the symmetry of the potential V_R , the electron wave functions will be even split across both atoms, hence we refer to that state as a delocalized state. Otherwise, each electron wave function will be supported on one particular atom in the molecule, in which case we call the electrons localized. We note here that we are considering the only the breaking of spatial symmetry of the wave functions among neutral spin minimizers (i.e., spin singlet configurations). We call the minimizer with the symmetry constraint, $\psi_+ = \psi_- = \psi_R$, a restricted minimizer to the energy functional, denoted as ψ_R . Thus

$$\begin{aligned} \psi_R &= \operatorname{argmin} \mathcal{E}_\alpha(\psi, \psi) \\ \text{s.t.} \quad & \int |\psi|^2 = 1. \end{aligned} \tag{6}$$

The unrestricted minimization on the other hand considers all possible ψ_+ and ψ_- with the normalization constraints. To distinguish, we denote the minimizers as ψ_\pm .

$$\begin{aligned} (\psi_+, \psi_-) &= \operatorname{argmin} \mathcal{E}_\alpha(\psi_+, \psi_-) \\ \text{s.t.} \quad & \int |\psi_+|^2 = \int |\psi_-|^2 = 1. \end{aligned} \tag{7}$$

Our goal in this work is to understand the symmetry breaking, i.e., the question whether $\psi_+ = \psi_- = \psi_R$. The following result gives the existence of minimizers to both (6) and (7).

Proposition 1.1. *For all $\alpha \geq 0$, there exist solutions $(\phi_+, \phi_-) \in H^1 \times H^1$ with $\int |\phi_\pm|^2 dx = 1$ such that*

$$\mathcal{E}_\alpha(\phi_+, \phi_-) = \min_{\psi_\pm \in H^1; \int |\psi_\pm|^2 dx = 1} \mathcal{E}_\alpha(\psi_+, \psi_-).$$

For a proof of this proposition, we refer the reader to the Concentration Compactness tools employed in [3, Theorem 1] or specifically for LDA models the recent work of [28], where a general existence theory is addressed for LDA models of this type with neutral or positive charge.

For the energy functional (3), we have two parameters R and α in the functional. We expect the following behavior of the minimizers for different ranges of parameters:

1. For $\alpha = 0$ and any $R > 0$, the minimizer have the symmetry $\psi_+ = \psi_- = \psi_R$.
2. Fix $R \geq 0$, when we increase α from 0: The minimizer is initially symmetric (hence it is continuous at $\alpha = 0$), the symmetry is broken for larger α ($\psi_+ \neq \psi_-$). The critical parameter α for the transition from symmetric to asymmetric minimizer depends on R .
3. Fix $\alpha > 0$, for R sufficiently large, the minimizer is asymmetric.

Therefore, this suggests a two-dimensional phase diagram where the axes are R and α with a phase transition from symmetric to asymmetric minimizers. In the current manuscript, we will fix R and vary the parameter α in our analysis in order to prove that symmetry breaking occurs in the α parameter as predicted. However, we will demonstrate the (α, R) phase diagram numerically and hence lend numerical support to the conjectured behaviors in R . Some technical difficulties arise in the the analysis when varying R in particular when taking $R \rightarrow \infty$, which we comment on in Section 5 and plan to address in future work. We make our statements precise in the following theorems.

Theorem 1. Fix $R > 0$, denote ψ_R the minimizer of (6) and ψ_{\pm} the minimizer of (7), we have $\psi_{\pm} = \psi_R$ for $\alpha \ll 1$, and $\psi_+ \neq \psi_-$ for $\alpha \gg 1$.

In other words, as we increase α , the symmetry $\psi_+ = \psi_-$ is broken. In fact, we can give a more precise characterization of the minimizer ψ_{\pm} as $\alpha \rightarrow \infty$.

Theorem 2. Fix $R > 0$, as $\alpha \rightarrow \infty$, up to symmetries of the equation, the rescaled and translated minimizer of (7)

$$\alpha^{-\frac{3}{2}} \psi_{\pm}(\alpha^{-1}(x \mp R e_1)) \quad (8)$$

converges to ϕ in H^1 , where ϕ is the unique positive, radial solution to the equation

$$-\frac{1}{2} \Delta \phi - \frac{4}{3} |\phi|^{\frac{2}{3}} \phi + E \phi = 0, \text{ with } \int |\phi|^2 dx = 1. \quad (9)$$

This can also be seen as the constrained minimizer of the Lagrangian

$$\mathcal{E}_s(\phi) = \frac{1}{2} \int |\nabla \phi|^2 dx - \int |\phi|^{8/3} dx, \quad (10)$$

with mass $\int |\phi|^2 dx = 1$. In other words, as $\alpha \rightarrow \infty$, each electron becomes concentrated over a different nucleus.

Our results in the small α setting rely heavily on the results of Lieb, Lions and others relating to the concentration compactness phenomenon for constructing minimizers of constrained Lagrangians at $\alpha = 0$, then an application of the Implicit Function Theorem for small α . Our result for large α on the other hand follows from essentially comparing the variational problem to a scale-invariant semi-linear problem, which in turn relies strongly on the orbital stability of solitons for the unperturbed Dirac non-linearity in 3 dimensions, $|u|^{\frac{2}{3}} u$.

The proof for the small α regime is presented in Section 2, while the large α regime is treated in Section 3. We present the analysis in detail for fixed $R > 0$ and varying α throughout the proof. Without loss of generality, for our analysis we will assume $R = 1$ and denote $V = V_R$. Detailed numerical studies of the (α, R) phase diagram and in particular the transition between small and large α for fixed R are discussed in Section 4. Concluding remarks and a discussion of the analysis in the case of varying R are included in Section 5. The numerical methods are presented in Appendix A using a finite element package developed by the group of the first author and implemented in the thesis of the second author to study variational problems in electronic structure theory.

2 Proof in the small α regime

2.1 The restricted Hartree model: Case $\alpha = 0$

When $\alpha = 0$, the energy functional we consider becomes

$$\mathcal{E}_0(\psi_+, \psi_-) = \frac{1}{2} \int |\nabla \psi_+|^2 dx + \frac{1}{2} \int |\nabla \psi_-|^2 dx + \int V(x) \rho(x) dx + \frac{1}{2} \iint \frac{\rho(x) \rho(y)}{|x-y|} dx dy. \quad (11)$$

Without the exchange-correlation energy, the minimizer is always symmetric. Indeed, fixing any density ρ with $\int \rho = 2$, we have

$$\mathcal{E}_0(\sqrt{\rho}/\sqrt{2}, \sqrt{\rho}/\sqrt{2}) = \inf\{\mathcal{E}_0(\psi_+, \psi_-) \mid |\psi_+|^2 + |\psi_-|^2 = \rho\}. \quad (12)$$

Define $\rho_+ = |\psi_+|^2$ and $\rho_- = |\psi_-|^2$, the above follows from the convexity

$$2 \int \left| \nabla \sqrt{(\rho_+ + \rho_-)/2} \right|^2 dx \leq \int |\nabla \sqrt{\rho_+}|^2 dx + \int |\nabla \sqrt{\rho_-}|^2 dx, \quad (13)$$

and the equality holds if and only if $\rho_+ = \rho_-$ (see [42, Page 177, Theorem 7.8]). Thus, we may denote the common orbital function as $\phi = \psi_+ = \psi_-$, which minimizes the functional

$$\mathcal{E}_0(\phi) = \int |\nabla \phi|^2 dx + 2 \int V(x) |\phi|^2 dx + 2 \iint \frac{|\phi(x)|^2 |\phi(y)|^2}{|x-y|} dx dy. \quad (14)$$

Note that this functional has the same form as the restricted Hartree model treated in [44, Theorem II.2], which guarantees the existence of a minimizer. Moreover, the minimizer is non-negative without loss of generality and satisfies the Euler-Lagrange equation

$$-\frac{1}{2} \Delta \phi + E_0 \phi + V \phi + 2(v_c * |\phi|^2) \phi = 0 \quad (15)$$

where $v_c(x) = |x|^{-1}$ denotes the Coulomb kernel and $E_0 \geq 0$ is the Lagrange multiplier. We now show that E_0 must be strictly positive. Suppose $E_0 = 0$, define $W := V + 2v_c * |\phi|^2$, we have

$$-\frac{1}{2} \Delta \phi + W \phi = 0. \quad (16)$$

Using Newton's theorem, the spherical average of W , denoted by \bar{W} is non-positive outside the ball B_R (since the ball contains all the nuclei charge). Thus, we get trivially that the positive part of $\bar{W}_+ = \max\{\bar{W}, 0\} \in L^{3/2}(B_R^c)$. This implies that $\phi \notin L^2(B_R^c)$ by [41, Lemma 7.18], which is clearly a contradiction, since $\int |\phi|^2 = 1$. Therefore, $E_0 > 0$. This implies that the nuclear potential is properly binding in a similar sense to that explored in [58].

For a purpose that will be clear later, we also consider the variational problem (14) with more general mass constraints and denote the minimum as I_M :

$$\begin{aligned} I_M &:= \inf \left\{ \mathcal{E}_0(\phi) \mid \int |\phi|^2 = M/2 \right\} \\ &= \inf \left\{ \mathcal{E}_0(\phi) \mid \int |\phi|^2 \leq M/2 \right\} \\ &= \inf \left\{ \mathcal{E}_0(\sqrt{\rho}/\sqrt{2}) \mid \int \rho \leq M \right\}, \end{aligned} \quad (17)$$

where the second equality follows from the fact that I_M is monotonically decreasing in M as we can always put some excessive charge far away from the nuclei with negligible contribution to the energy. Furthermore, I_M is strictly convex for $M \in [0, M_c)$ for some $M_c \geq 2$, which follows the standard convexity argument applies to $\mathcal{E}_0(\sqrt{\rho}/\sqrt{2})$ as in the proof of parts (iii) and (iv) of [44, Corollary II.1] (see also the proof of convexity of the energy of the related Thomas-Fermi-von Weizsäcker theory in [8]). We also have the relation

$$\left. \frac{\partial I_M}{\partial M} \right|_{M=2} = -E_0 < 0, \quad (18)$$

since E_0 is the Lagrange multiplier corresponding to the constraint $\int |\phi|^2 = M/2$. This in turn guarantees that $M_c > 2$, as in Part (i) of [44, Corollary II.1]. Therefore, denote $E_0(M)$ the corresponding Lagrange multiplier for I_M , we arrive at

$$-\left. \frac{\partial E_0(M)}{\partial M} \right|_{M=2} = \left. \frac{\partial^2 I_M}{\partial M^2} \right|_{M=2} > 0. \quad (19)$$

Following the analysis of [43, Theorem 3.1] using elliptic estimates, one observes that if $\phi \in H^1$ is a solution to (15), then $\phi \in H^2$.

2.2 Implicit function theorem analysis for small α

We consider (3) for α small. First of all, by restricting to the class of solutions symmetric with respect to reflection in x , we know there exists a delocalized solution obeying the correct symmetry properties. For $\alpha = 0$, (3) is a convex functional and there exists a *unique* delocalized solution $\psi_+ = \psi_- = \phi$ such that $\|\phi\|_{L^2} = 1$. The following result extends the uniqueness to small α . This result is similar to one proved in [39] for the Thomas-Fermi-Dirac-von Weizsäcker model.

Proposition 2.1. *For $\alpha \geq 0$ sufficiently small, there exists a unique, delocalized minimizer to (3) such that $\psi_+ = \psi_- = \phi$ with $\|\phi\|_{L^2} = 1$. The dependence upon α is C^1 .*

The remainder of this section is devoted to the proof of Proposition 2.1. The idea is to construct a symmetric solution branch stemming from the unique solution at $\alpha = 0$ that comes from the convexity of the energy functional in that limit. While the positive α perturbation is non-convex, the Euler-Lagrange equations can be solved using a Lyapunov-Schmidt reduction. In fact, we will see that we can construct an implicit function theorem argument using the convexity at $\alpha = 0$ and in doing so, that locally only the symmetric branch will be possible. First, we will allow the branch to vary with respect to mass, then we will fix the Lagrange multipliers E_+ and E_- (in most cases we will observe $E_+ = E_-$) as a function of α to guarantee the mass 1 electron branch.

The Euler-Lagrange equations for \mathcal{E}_α can be written as the following with F defined as a function on $(H^2)^2 \times \mathbb{R}^3$

$$F(\psi_+, \psi_-; \alpha, E_+, E_-) := \begin{pmatrix} -\frac{1}{2}\Delta\psi_+ + E_+\psi_+ + V\psi_+ + (v_c * (|\psi_+|^2 + |\psi_-|^2))\psi_+ - \frac{4}{3}\alpha|\psi_+|^{\frac{2}{3}}\psi_+ \\ -\frac{1}{2}\Delta\psi_- + E_-\psi_- + V\psi_- + (v_c * (|\psi_+|^2 + |\psi_-|^2))\psi_- - \frac{4}{3}\alpha|\psi_-|^{\frac{2}{3}}\psi_- \end{pmatrix} = 0. \quad (20)$$

To apply the Lyapunov-Schmidt reduction, we need to address the kernel of the Jacobian with respect to ψ_\pm for the Euler-Lagrange equations. This is given by the operator

$$D_\psi F(\psi_+, \psi_-; \alpha, E_+, E_-) \begin{pmatrix} f_+ \\ f_- \end{pmatrix} = \begin{pmatrix} L_+ f_+ + 2\psi_+ v_c * (\psi_- \bar{f}_-) \\ L_- f_- + 2\psi_- v_c * (\psi_+ \bar{f}_+) \end{pmatrix} \quad (21)$$

for

$$\begin{aligned} L_+(\psi_\pm; \alpha, E_+) f_+ &:= \left(-\frac{1}{2}\Delta + E_+ + V + v_c * (|\psi_+|^2 + |\psi_-|^2) - \frac{20}{9}\alpha|\psi_+|^{\frac{2}{3}} \right) f_+ + 2\psi_+ v_c * (\psi_+ \bar{f}_+); \\ L_-(\psi_\pm; \alpha, E_-) f_- &:= \left(-\frac{1}{2}\Delta + E_- + V + v_c * (|\psi_+|^2 + |\psi_-|^2) - \frac{20}{9}\alpha|\psi_-|^{\frac{2}{3}} \right) f_- + 2\psi_- v_c * (\psi_- \bar{f}_-). \end{aligned}$$

For $\psi_+ = \psi_- = \phi$, the unique solution at $\alpha = 0$ with resulting Lagrange multiplier E_0 stemming from the convexity of \mathcal{E}_0 , we have

$$D_\psi F(\phi, \phi; 0, E_0, E_0) \begin{pmatrix} f_+ \\ f_- \end{pmatrix} = \begin{pmatrix} L_{\phi, E_0} f_+ + 2\phi v_c * (\phi \bar{f}_-) \\ L_{\phi, E_0} f_- + 2\phi v_c * (\phi \bar{f}_+) \end{pmatrix}$$

for

$$L_{\phi, E_0} f = \left(-\frac{1}{2}\Delta + E_0 + V + 2v_c * |\phi|^2 \right) f + 2\phi v_c * (\phi \bar{f}).$$

In the class of symmetric solutions, the problem reduces to solving a scalar equation instead of a system of equations.

2.3 Analysis of the linearized operators for $\alpha = 0$

We prove here that at $\alpha = 0$, $\psi_+ = \psi_- = \phi$, $E = E_0$, then the linearized operator has a kernel, but it can only lead to solutions where ψ_+ and ψ_- take on different masses. This is a key step in applying the implicit function theorem in α locally. To see this, we linearize (15) to get the operator

$$\tilde{L}_{\phi, E_0} f = \left(-\frac{1}{2} \Delta + E_0 + V + 2v_c * |\phi|^2 \right) f + 4\phi v_c * (\phi \bar{f}). \quad (22)$$

We observe that the operator \tilde{L}_{ϕ, E_0} can be written in the form

$$\tilde{L}_{\phi, E_0} = -\frac{1}{2} \Delta + E_0 + V + V_\phi + W_\phi,$$

where

$$V_\phi := 2v_c * |\phi|^2$$

is a potential with $1/|x|$ decay and

$$W_\phi f := 4\phi v_c * (\phi \bar{f})$$

is a self-adjoint convolution operator, where we note that the function ϕ is exponentially decaying.

Since $V + V_\phi + W_\phi$ is a relatively compact perturbation, we observe that the continuous spectrum of \tilde{L}_{ϕ, E_0} is the interval $[E_0, \infty)$ by applying Weyl's Theorem, see [53, 42] for instance, or [40] where the functional analysis of Hartree-style equations is discussed in some detail.

Lemma 2.2. *The operator \tilde{L}_{ϕ, E_0} has only trivial kernel.*

Proof. Let us assume to the contrary there exists $f \in H^2$ such that

$$\tilde{L}_{\phi, E_0} f = 0.$$

Then, we observe that

$$0 = \left\langle \left(-\frac{1}{2} \Delta + E_0 + V + V_\phi \right) f, f \right\rangle + \langle W_\phi f, f \rangle.$$

Given the structure of W_ϕ and the nature of the state ϕ , we have that

$$\langle W_\phi f, f \rangle > 0 \text{ for } f \neq 0,$$

since the Coulomb kernel is strictly positive, which is easily seen from the Fourier representation.

Taking the orthogonal decomposition $f = c\phi + \phi^\perp$ and using that ϕ is the unique kernel of the operator $L_- = -\frac{1}{2} \Delta + E_0 + V + V_\phi$, where the notation L_- here is chosen to match that of the semilinear literature for linearized operators about nonlinear states, see for instance [40]. Hence if $\phi^\perp \neq 0$, we have a contradiction immediately from the coercivity of the operator L_- . Thus, it remains the possibility that $f = c\phi$. However if $c \neq 0$, we have $\langle W_\phi f, f \rangle > 0$, and therefore $f = 0$. \square

Remark 2.1. This is a similar strategy to that of standard semi-linear problems, however in such a case the perturbation of the L_- operator is negative in total and hence the spectral theory of the linearized operator must be understood in much greater detail. Here, the perturbation is actually positive, so the arguments are greatly simplified. Also, we have a potential V here, which has broken the translation invariance and hence we do not need to consider a 1-parameter family of functions, but just a single ϕ in the kernel of L_- .

2.4 Construction of solutions near $\alpha = 0$

Proposition 2.3. *The Jacobian $D_\psi F(\phi, \phi; 0, E_0, E_0)$ as defined in (21) has kernel given by $\text{span}\{(\phi, -\phi)\}$. As a result, there exists a unique C^1 path of solutions in (α, E_+, E_-) for the equation (20) with fixed constraint $\|\psi_\pm\|_{L^2} = 1$ in $H^2 \times H^2$. Moreover, the unique solution satisfies the symmetry $\psi_+ = \psi_-$.*

Proof. We must study the invertibility of $D_\psi F$ at $\alpha = 0$. In the restricted space, $\psi_+ = \psi_-$, the invertibility is established in Lemma 2.2 through the invertibility of \tilde{L}_{ϕ, E_0} . More generally, let us consider (f_1, f_2) that solves $D_\psi F(f_1, f_2)^\top = 0$, then $\tilde{L}_{\phi, E_0}(f_1 + f_2) = 0$. Hence, either $f_1 + f_2$ is a non-trivial kernel function of \tilde{L}_{ϕ, E_0} (which is excluded by Lemma 2.2) or $f_1 = -f_2 = f$ and f is a non-trivial kernel function for a modified operator

$$\mathcal{L}_{\phi, E_0} f = \left(-\frac{1}{2} \Delta + E_0 + V + 2v_c * |\phi|^2 \right) f,$$

which through the equation satisfies $\mathcal{L}_{\phi, E_0} \phi = 0$. Since $\phi > 0$, it is the ground state and simple. Therefore the kernel of $D_\psi F(\phi, \phi; 0, E_0, E_0)$ is one dimensional and described completely as $\text{span}\{(\phi, -\phi)\}$.

The remaining proof relies on varying E_\pm using the standard Lyapunov-Schmidt construction of $\psi_\pm(E, \alpha)$ solving the Euler-Lagrange equation, see [37, Proposition 1] for a general discussion of the method. We write

$$(\psi_+, \psi_-) = (\phi, \phi) + c_0(\phi, -\phi) + (\eta_+, -\eta_-),$$

for $c_0 \sim \sqrt{\alpha}$ and $\int (\eta_+ + \eta_-) \phi \, dx = 0$. We claim that

$$\|\eta_\pm(c_0, E_\pm - E_0, \alpha)\|_{H^2} \lesssim c_0^2, \quad |E_\pm - E_0| \lesssim c_0^2,$$

where the dependence of η_\pm upon our bifurcating parameters have been made explicit and in particular we have shifted the dependence upon E_\pm to that $E_\pm - E_0$ such that $\eta(0, 0, 0) = 0$ for simplicity. Indeed, expanding (20) about (ϕ, ϕ) in this fashion we have

$$F(\phi, \phi; 0, E_0, E_0) + D_\psi F(\phi, \phi; 0, E_\pm) \begin{pmatrix} \eta_+ \\ \eta_- \end{pmatrix} + \mathcal{R}(\eta, c_0, \alpha, E_\pm - E_0, \phi) = \begin{pmatrix} 0 \\ 0 \end{pmatrix}, \quad (23)$$

where the remainder term $\mathcal{R}(\eta, c_0, \alpha, E_\pm - E_0, \phi)$ will be specified below and satisfies

$$|\mathcal{R}| \leq C(|\eta|^2 + c_0^2 + \alpha + (E_\pm - E_0)).$$

We note here that the linearization is $D_\psi F(\phi, \phi; 0, E_\pm)$ and not $D_\psi F(\phi, \phi; 0, E_0, E_0)$. Using the properties of $D_\psi F$, ϕ and E_0 , we then observe that we can first re-write the equation for

$$(\eta_+, \eta_-) = (\eta_+, \eta_-)(c_0, E_\pm - E_0, \alpha)$$

as

$$\begin{pmatrix} \eta_+ \\ \eta_- \end{pmatrix} = (P^\perp D_\psi F(\phi, \phi; 0, E_\pm) P^\perp)^{-1} P^\perp \mathcal{R}(\eta, c_0, \alpha, E_\pm - E_0), \quad (24)$$

where $P^\perp \vec{f} = \vec{f} - \langle \vec{f}, (\phi, -\phi)^\top \rangle (\phi, -\phi)^\top$ for $\vec{f} = (f_1, f_2)^\top$ projects to the orthogonal complement of the kernel of $D_\psi F(\phi, \phi, 0, E_0, E_0)$. This implies that (23) can be written as

$$\begin{aligned} \left(-\frac{1}{2} \Delta + E_\pm + V \right) \eta_\pm &= (E_\pm - E_0) \phi + c_0 (E_\pm - E_0) \phi - \alpha |\phi| (1 \pm c_0) + \eta_\pm^{\frac{2}{3}} (\phi (1 \pm c_0) + \eta_\pm) \\ &+ v_c * \left[2c_0^2 \phi^2 + 2(1 + c_0) \phi \eta_+ + 2(1 - c_0) \phi \eta_- + \eta_+^2 + \eta_-^2 \right] \phi \\ &\pm c_0 v_c * \left[2c_0^2 \phi^2 + 2(1 + c_0) \phi \eta_+ + 2(1 - c_0) \phi \eta_- + \eta_+^2 + \eta_-^2 \right] \phi \\ &+ v_c * \left[2\phi^2 + 2c_0^2 \phi^2 + 2(1 + c_0) \phi \eta_+ + 2(1 - c_0) \phi \eta_- + \eta_+^2 + \eta_-^2 \right] \eta_\pm. \end{aligned}$$

As we are taking $|E_{\pm} - E_0|$ small, $P^{\perp} D_{\psi} F(\phi, \phi; 0, E_{\pm}) P^{\perp}$ is invertible since $P^{\perp} D_{\psi} F(\phi, \phi; 0, E_0) P^{\perp}$ is invertible. We observe that by the Implicit Function Theorem there exists a solution $\vec{\eta} = (\eta_-, \eta_+)$ such that

$$\|\vec{\eta}\|_{H^2} \leq C(c_0^2 + \alpha + |E_+ - E_0| + |E_- - E_0|). \quad (25)$$

Projecting (23) onto $(\phi, -\phi)$, we compute directly that¹

$$(E_+ - E_0) - (E_- - E_0) + c_0[(E_+ - E_0) + (E_- - E_0)] + \mathcal{O}\left(\|\vec{\eta}\|_{L^2}^2 + c_0^3 + \alpha(c_0 + \|\vec{\eta}\|_{L^2}^{\frac{5}{3}})\right) = 0, \quad (26)$$

where we have implicitly used uniform Sobolev bounds on ϕ and the smallness of c_0 , α and $E_{\pm} - E_0$. This allows us to use the Implicit Function Theorem once again to solve for E_+ given E_- and observe that

$$|E_+ - E_0| \leq C(c_0^3 + \alpha c_0 + \alpha^{\frac{5}{3}} + |E_- - E_0|),$$

where we have plugged in the bound on $\|\eta\|_{L^2}$ from (25). Now, using the two constraint equations for the mass, we have

$$\int (2c_0\phi + c_0^2\phi^2 + 2(1 + c_0)\phi\eta_+ + \eta_+^2) dx = 0 \quad (27)$$

and

$$\int (-2c_0\phi + c_0^2\phi^2 + 2(1 - c_0)\phi\eta_- + \eta_-^2) dx = 0. \quad (28)$$

Using the linear combination (27) + (28) and the orthogonality of (η_+, η_-) to (ϕ, ϕ) as constructed, we first observe by plugging the resulting implicit bound on $\|\vec{\eta}\|_{L^2} \leq Cc_0^2$ in (26) that

$$|E_- - E_0| \leq C(\alpha + c_0^2),$$

which implies for the linear combination (27) - (28), we can observe that

$$c_0^2 \leq C\alpha.$$

Once the overall dependence upon α has been determined, we realize that on the branch described above in (27) and (28), everything is indeed higher order to the $\mathcal{O}(c_0)$ term. Thus, $c_0 = 0$ lest we move off the mass 1 branch. Therefore, we have $\psi_+ = \psi_-$ for sufficiently small α . \square

Remark 2.2. We note that the nature of the kernel of $D_{\psi} F$ is not so surprising at $\alpha = 0$, as a major symmetry of \mathcal{E}_0 would be to multiply (ψ_+, ψ_-) by a rotation matrix, which is an invariant of the Lagrangian. However, given that at $\alpha = 0$, we have $\psi_+ = \psi_- = \phi$, this symmetry generates no new solutions except the one we have found in the kernel. Using the convexity of \mathcal{E}_0 , we have uniqueness of the symmetric solution ϕ as a minimizer having fixed mass $\|\phi\|_{L^2} = 1$.

Remark 2.3. From the sign changes (27) and (28), we expect that with no mass constraint the branch construction stemming from the kernel of $D_{\psi} F$ to leading order leads to $E_+ = -E_-$. If we were allowed to make such a symmetric reduction, the arguments above can be simplified.

¹Here, we use the following bound pointed out to the authors by N. Visciglia: Let $\alpha > 0$ be given. Then for every $a, b \in \mathbb{C}$ we have the following inequality:

$$|(a+b)|a+b|^{\alpha} - a|a|^{\alpha} - b|b|^{\alpha}| \lesssim (|a||b|^{\alpha} + |b||a|^{\alpha}).$$

2.5 Construction of the local branch under the symmetry assumption

In Proposition 2.3 above, we established that the bifurcation off $\alpha = 0$ occurs in the symmetry class such that $\psi_+ = \psi_-$. Within this symmetry class, we demonstrate in this section that one may construct a unique local branch of solutions that preserves the mass of the electronic states as 1. We could have absorbed this constraint above in a modification of the application of the implicit function theorem, but for simplicity of exposition we have split the two arguments apart.

Using that the linearization preserve the symmetry of solutions proven in Proposition 2.3, let us limit ourselves to solutions of the simplified Euler-Lagrange equation for $\phi(E, \alpha)$ given by

$$-\frac{1}{2}\Delta\phi(x) + E\phi(x) - V(x)\phi(x) + 2 \int \frac{|\phi|^2(y)}{|x-y|} dy \phi(x) - \alpha|\phi(x)|^{\frac{2}{3}}\phi(x) = 0.$$

Denote the mass of ϕ by

$$M(E, \alpha) := \int |\phi(E, \alpha)|^2 dx.$$

By construction, $M(E_0, 0) = 1$. To find mass 1 states, using that $\phi = \phi(E, \alpha)$, we wish to find $E(\alpha)$ solving

$$M(E, \alpha) = \int |\phi(E(\alpha), \alpha)|^2 dx - 1 = 0.$$

Hence, we apply the Implicit Function Theorem once more, which guarantees the solvability of $E(\alpha)$ provided

$$\left. \frac{\partial M}{\partial E} \right|_{E=E_0, \alpha=0} \neq 0.$$

However, at $\alpha = 0$ this follows directly from (19). Using the Implicit Function Theorem for a small range of α , there is an $E = E(\alpha)$ satisfying the mass constraint. Thus the proof of Proposition 2.1 is complete.

3 Localization and symmetry breaking for large α

In this section, we prove Theorem 2 by classifying the large α behavior of the minimizer.

3.1 A priori energy estimate

We consider a variational problem with only the kinetic and exchange terms:

$$\min_{\varphi: \int |\varphi|^2 = 1} \mathcal{F}(\varphi) = \frac{1}{2} \int |\nabla \varphi|^2 - \int |\varphi|^{8/3}. \quad (29)$$

It is now classical in the theory of nonlinear Schrödinger equations that the minimizer of (29) exists. In fact, there is a unique radial minimizer, and all minimizers are translated versions of it, see for instance [60]. Denote φ the radial minimizer of (29) centered at zero, it satisfies

$$-\frac{1}{2}\Delta\varphi - \frac{4}{3}|\varphi|^{2/3}\varphi + E\varphi = 0 \quad (30)$$

with E being a strictly positive Lagrange multiplier. Moreover, φ decays exponentially as $|x| \rightarrow \infty$.

We consider dilation operator D_α for $\alpha > 0$ that preserves the L^2 norm

$$(D_\alpha f)(x) = \alpha^{3/2} f(\alpha x). \quad (31)$$

Let x_+ and x_- minimize

$$\min\left(\|\nabla\psi_{\pm} - \nabla(D_{\alpha}\varphi)(\cdot - x_{\pm})\|_{L^2}^2 + E\|\psi_{\pm} - (D_{\alpha}\varphi)(\cdot - x_{\pm})\|_{L^2}^2\right). \quad (32)$$

We write the remainder as

$$\psi_{\pm} = (D_{\alpha}(\varphi + w_{\pm}))(\cdot - x_{\pm}). \quad (33)$$

Correspondingly, we have $\varphi = D_{\alpha}^{-1}\tau_{x_{\pm}}^{-1}(\psi_{\pm}) - w_{\pm}$, to simplify notation, we denote

$$\tilde{\psi}_{\pm} = D_{\alpha}^{-1}\tau_{x_{\pm}}^{-1}\psi_{\pm} = \alpha^{-3/2}\psi_{\pm}\left(\frac{x + x_{\pm}}{\alpha}\right). \quad (34)$$

As $\{\psi_{\pm}\}$ minimize \mathcal{E}_{α} , we have

$$\begin{aligned} 0 &\leq \mathcal{E}_{\alpha}((D_{\alpha}\varphi)(\cdot - x_+), (D_{\alpha}\varphi)(\cdot - x_-)) - \mathcal{E}_{\alpha}(\psi_+, \psi_-) \\ &= \alpha^2(2\mathcal{F}(\varphi) - \mathcal{F}(\tilde{\psi}_+) - \mathcal{F}(\tilde{\psi}_-)) + \int V(\rho_{\varphi} - \rho_{\psi}) \\ &\quad + \frac{1}{2} \iint \frac{\rho_{\varphi}(x)\rho_{\varphi}(y)}{|x-y|} dx dy - \frac{1}{2} \iint \frac{\rho_{\psi}(x)\rho_{\psi}(y)}{|x-y|} dx dy, \end{aligned} \quad (35)$$

where we have set

$$\rho_{\varphi}(x) = |(D_{\alpha}\varphi)(x - x_+)|^2 + |(D_{\alpha}\varphi)(x - x_-)|^2. \quad (36)$$

Note that $\frac{1}{2} \iint \frac{\rho_{\psi}(x)\rho_{\psi}(y)}{|x-y|} dx dy \geq 0$ and $\int V\rho_{\varphi} \leq 0$, rearranging the terms, we obtain

$$\mathcal{F}(\tilde{\psi}_+) + \mathcal{F}(\tilde{\psi}_-) - 2\mathcal{F}(\varphi) \leq \frac{1}{\alpha^2} \frac{1}{2} \iint \frac{\rho_{\varphi}(x)\rho_{\varphi}(y)}{|x-y|} dx dy - \frac{1}{\alpha^2} \int V\rho_{\psi} dx. \quad (37)$$

For the first term on the right hand side, we have by the definition of ρ_{φ} in (36) that

$$\begin{aligned} \frac{1}{2} \iint \frac{\rho_{\varphi}(x)\rho_{\varphi}(y)}{|x-y|} &= \frac{1}{2} \iint \frac{(|(D_{\alpha}\varphi)(x - x_+)|^2 + |(D_{\alpha}\varphi)(x - x_-)|^2)(|(D_{\alpha}\varphi)(y - x_+)|^2 + |(D_{\alpha}\varphi)(y - x_-)|^2)}{|x-y|} \\ &\leq \iint \frac{|(D_{\alpha}\varphi)(x - x_+)|^2 |(D_{\alpha}\varphi)(y - x_+)|^2}{|x-y|} + \iint \frac{|(D_{\alpha}\varphi)(x - x_-)|^2 |(D_{\alpha}\varphi)(y - x_-)|^2}{|x-y|} \\ &= 2 \iint \frac{|(D_{\alpha}\varphi)(x)|^2 |(D_{\alpha}\varphi)(y)|^2}{|x-y|} \\ &= 2\alpha \iint \frac{|\varphi(x)|^2 |\varphi(y)|^2}{|x-y|}, \end{aligned} \quad (38)$$

where we have used the scaling relation of D_{α} and change of variables $\alpha x \mapsto x, \alpha y \mapsto y$ in the last equality. To control the second term on the right hand side of (37), recall that by Hardy's uncertainty principle, we have for any $X \in \mathbb{R}^3$ and $f \in H^1$

$$\int \frac{1}{|x-X|} |f(x)|^2 dx \leq 4\|f\| \|\nabla f\|. \quad (39)$$

Therefore, since $\|\psi_{\pm}\| = 1$, we have

$$-\int V\rho_{\psi} dx = \int \frac{1}{|x-e_1|} (|\psi_+|^2 + |\psi_-|^2) dx + \int \frac{1}{|x+e_1|} (|\psi_+|^2 + |\psi_-|^2) dx \leq C(\|\nabla\psi_-\| + \|\nabla\psi_+\|). \quad (40)$$

Thus, we arrive at

$$\begin{aligned}
\mathcal{F}(\tilde{\psi}_+) + \mathcal{F}(\tilde{\psi}_-) - 2\mathcal{F}(\varphi) &\leq \frac{C}{\alpha} + \frac{C}{\alpha^2} (\|\nabla\psi_+\| + \|\nabla\psi_-\|) \\
&\leq \frac{C}{\alpha} + \frac{C}{\alpha^2} (\|\nabla D_\alpha(\varphi + w_+)\| + \|\nabla D_\alpha(\varphi + w_-)\|) \\
&\leq \frac{C}{\alpha} + \frac{C}{\alpha} (\|\nabla w_+\| + \|\nabla w_-\|) \\
&\leq \frac{C}{\alpha} + \frac{C}{\alpha} (\|\nabla w_+\|^2 + \|\nabla w_-\|^2).
\end{aligned} \tag{41}$$

Using the result in [65] for the semilinear functional (29), the left hand side of (41) is bounded from below as

$$\mathcal{F}(\tilde{\psi}_+) + \mathcal{F}(\tilde{\psi}_-) - 2\mathcal{F}(\varphi) \geq g(\|w_+\|_{H^1}) + g(\|w_-\|_{H^1}), \tag{42}$$

where

$$g(t) = ct^2(1 - at^\theta - bt^4) \quad \text{with } a, b, c, \theta > 0. \tag{43}$$

Combining (41) and (42), we conclude that

$$\lim_{\alpha \rightarrow \infty} \|w_\pm\|_{H^1} = \lim_{\alpha \rightarrow \infty} \|\tilde{\psi}_\pm - \varphi\|_{H^1} = 0. \tag{44}$$

In other words, up to translation and dilation, the minimizer of (7) is close to the minimizer of the semilinear problem (29) for α large. This establishes the H^1 convergence stated in Theorem 2. We now proceed to establish the exact structure of the minimizer as stated in (8).

3.2 Location optimization

We further determine the translation vectors x_\pm . We claim that as $\alpha \rightarrow \infty$, the translation vectors $x_\pm \rightarrow \pm e_1$ (up to swapping x_+ and x_- , recall that swapping ψ_+ and ψ_- does not change the energy). The key observation is that the kinetic and exchange energy terms are invariant with respect to translation, and hence x_\pm are determined by the potential and Coulomb repulsion terms, which are higher order terms when α is large.

For this, we consider shifted minimizers

$$\hat{\psi}_+ = \psi_+(\cdot + e_1 + x_+) \quad \text{and} \quad \hat{\psi}_- = \psi_-(\cdot - e_1 + x_-). \tag{45}$$

By (33), we have

$$\hat{\psi}_\pm = (D_\alpha\varphi)(\cdot \pm e_1) + (D_\alpha w_\pm)(\cdot \pm e_1). \tag{46}$$

Due to minimality, we have

$$\begin{aligned}
0 &\leq \mathcal{E}_\alpha(\hat{\psi}_+, \hat{\psi}_-) - \mathcal{E}_\alpha(\psi_+, \psi_-) \\
&= \int V(\rho_{\hat{\psi}} - \rho_\psi) + \frac{1}{2} \iint \frac{\rho_{\hat{\psi}}(x)\rho_{\hat{\psi}}(y)}{|x-y|} dx dy - \frac{1}{2} \iint \frac{\rho_\psi(x)\rho_\psi(y)}{|x-y|} dx dy.
\end{aligned} \tag{47}$$

Recall ρ_φ and similarly define $\rho_{\hat{\varphi}}$ as

$$\begin{aligned}
\rho_\varphi(x) &= |(D_\alpha\varphi)(x - x_+)|^2 + |(D_\alpha\varphi)(x - x_-)|^2; \\
\rho_{\hat{\varphi}}(x) &= |(D_\alpha\varphi)(x + e_1)|^2 + |(D_\alpha\varphi)(x - e_1)|^2.
\end{aligned}$$

Denoting

$$\delta_{\text{VC}}(\rho_1, \rho_2) = \int V(\rho_1 - \rho_2) + \frac{1}{2} \iint \frac{\rho_1(x)\rho_1(y)}{|x-y|} dx dy - \frac{1}{2} \iint \frac{\rho_2(x)\rho_2(y)}{|x-y|} dx dy, \quad (48)$$

we rewrite (47) as

$$\delta_{\text{VC}}(\rho_{\widehat{\psi}}, \rho_{\psi}) = \delta_{\text{VC}}(\rho_{\widehat{\psi}}, \rho_{\widehat{\varphi}}) + \delta_{\text{VC}}(\rho_{\widehat{\varphi}}, \rho_{\varphi}) + \delta_{\text{VC}}(\rho_{\varphi}, \rho_{\psi}) \geq 0. \quad (49)$$

Let us estimate $\delta_{\text{VC}}(\rho_{\varphi}, \rho_{\psi})$ first. For the potential term, using (39) for $f = |\rho_{\varphi} - \rho_{\psi}|^{1/2}$,

$$\int |V(\rho_{\varphi} - \rho_{\psi})| \leq C \left\| |\rho_{\varphi} - \rho_{\psi}|^{1/2} \right\|_{L^2} \left\| \nabla |\rho_{\varphi} - \rho_{\psi}|^{1/2} \right\|_{L^2} \leq C \left\| \nabla |\rho_{\varphi} - \rho_{\psi}|^{1/2} \right\|_{L^2}. \quad (50)$$

For the difference in Coulomb energy

$$\begin{aligned} & \left| \frac{1}{2} \iint \frac{\rho_{\varphi}(x)\rho_{\varphi}(y)}{|x-y|} dx dy - \frac{1}{2} \iint \frac{\rho_{\psi}(x)\rho_{\psi}(y)}{|x-y|} dx dy \right| \\ & \leq \iint \frac{|\rho_{\varphi} - \rho_{\psi}|(x)\rho_{\varphi}(y)}{|x-y|} dx dy + \frac{1}{2} \iint \frac{(\rho_{\varphi} - \rho_{\psi})(x)(\rho_{\varphi} - \rho_{\psi})(y)}{|x-y|} dx dy \\ & \leq C \left\| \rho_{\varphi} - \rho_{\psi} \right\|_{L^{3/2}} \left\| \rho_{\varphi} \right\|_{L^1} + C \left\| \rho_{\varphi} - \rho_{\psi} \right\|_{L^{6/5}}^2, \end{aligned} \quad (51)$$

where the last line uses the Hardy-Littlewood-Sobolev inequality. Observe that using interpolation and Gagliardo-Nirenberg-Sobolev inequality, we have

$$\left\| f \right\|_{L^{6/5}} \leq \left\| f \right\|_{L^1}^{3/4} \left\| f \right\|_{L^3}^{1/4} \leq C \left\| f \right\|_{L^1}^{3/4} \left\| \nabla \sqrt{f} \right\|_{L^2}^{1/2}, \quad (52)$$

$$\left\| f \right\|_{L^{3/2}} \leq \left\| f \right\|_{L^1}^{1/2} \left\| f \right\|_{L^3}^{1/2} \leq C \left\| f \right\|_{L^1}^{1/2} \left\| \nabla \sqrt{f} \right\|_{L^2}. \quad (53)$$

Combined with the above three inequalities, we get

$$\left| \frac{1}{2} \iint \frac{\rho_{\varphi}(x)\rho_{\varphi}(y)}{|x-y|} dx dy - \frac{1}{2} \iint \frac{\rho_{\psi}(x)\rho_{\psi}(y)}{|x-y|} dx dy \right| \leq C \left\| \nabla |\rho_{\varphi} - \rho_{\psi}|^{1/2} \right\|_{L^2}. \quad (54)$$

To estimate the right hand side of (50) and (54), by definition

$$\begin{aligned} & \left\| \nabla |\rho_{\varphi} - \rho_{\psi}|^{1/2} \right\|_{L^2} \leq \left\| \nabla (2|D_{\alpha}\varphi||D_{\alpha}w_{+}| + 2|D_{\alpha}\varphi||D_{\alpha}w_{-}| + |D_{\alpha}w_{+}|^2 + |D_{\alpha}w_{-}|^2)^{1/2} \right\|_{L^2} \\ & \leq C \left(\left\| \nabla (|D_{\alpha}\varphi||D_{\alpha}w_{+}|) \right\|_{L^2} + \left\| \nabla (|D_{\alpha}\varphi||D_{\alpha}w_{-}|) \right\|_{L^2} \right. \\ & \quad \left. + \left\| \nabla |D_{\alpha}w_{+}| \right\|_{L^2} + \left\| \nabla |D_{\alpha}w_{-}| \right\|_{L^2} \right) \\ & \leq C\alpha (\|w_{+}\|_{H^1} + \|w_{-}\|_{H^1}), \end{aligned} \quad (55)$$

where we have used the convexity of $|\nabla \sqrt{\rho}|^2$ and the Cauchy-Schwarz inequality. Note that the α pre-factor on the right hand side is natural from the scaling, since the characteristic length scale of ρ_{φ} is order $1/\alpha$ due to the construction by dilation. Therefore, to sum up,

$$\left| \delta_{\text{VC}}(\rho_{\varphi}, \rho_{\psi}) \right| \leq C\alpha (\|w_{+}\|_{H^1} + \|w_{-}\|_{H^1}). \quad (56)$$

It is easy to check that the same upper bound also holds for $\delta_{\text{VC}}(\rho_{\hat{\varphi}}, \rho_{\varphi})$. Thus,

$$\delta_{\text{VC}}(\rho_{\hat{\varphi}}, \rho_{\varphi}) \geq -C\alpha(\|w_+\|_{H^1} + \|w_-\|_{H^1}). \quad (57)$$

We now turn the above estimate of the Coulomb energy difference into an estimate of the translation vectors x_{\pm} . For this, we calculate more explicitly $\delta_{\text{VC}}(\rho_{\hat{\varphi}}, \rho_{\varphi})$ (recall that φ is the unique radial minimizer to the semilinear functional (29)). We have

$$\begin{aligned} \delta_{\text{VC}}(\rho_{\varphi}, \rho_{\hat{\varphi}}) &= \int V(\rho_{\varphi} - \rho_{\hat{\varphi}}) + \iint \frac{|D_{\alpha}\varphi|^2(x-x_+)|D_{\alpha}\varphi|^2(y-x_-)}{|x-y|} dx dy \\ &\quad - \iint \frac{|D_{\alpha}\varphi|^2(x-x_+)|D_{\alpha}\varphi|^2(y-x_-)}{|x-y|} dx dy. \end{aligned} \quad (58)$$

As φ decays exponentially, we have

$$\iint \frac{|D_{\alpha}\varphi|^2(x-x_+)|D_{\alpha}\varphi|^2(y-x_-)}{|x-y|} dx dy \lesssim \frac{1}{\alpha}, \quad (59)$$

and therefore

$$\int V(\rho_{\varphi} - \rho_{\hat{\varphi}}) + \iint \frac{|D_{\alpha}\varphi|^2(x-x_+)|D_{\alpha}\varphi|^2(y-x_-)}{|x-y|} dx dy \leq C\alpha(\|w_+\|_{H^1} + \|w_-\|_{H^1}) + \mathcal{O}(\alpha^{-1}). \quad (60)$$

This implies

$$\begin{aligned} &\lim_{\alpha \rightarrow \infty} \frac{1}{\alpha} \int V(\rho_{\varphi} - \rho_{\hat{\varphi}}) \\ &= \lim_{\alpha \rightarrow \infty} -\frac{1}{\alpha} \int \left(\frac{1}{|x-e_1|} + \frac{1}{|x+e_1|} \right) (|D_{\alpha}\varphi|^2(x-x_+) - |D_{\alpha}\varphi|^2(x-e_1)) dx \\ &\quad + \lim_{\alpha \rightarrow \infty} -\frac{1}{\alpha} \int \left(\frac{1}{|x-e_1|} + \frac{1}{|x+e_1|} \right) (|D_{\alpha}\varphi|^2(x-x_-) - |D_{\alpha}\varphi|^2(x+e_1)) dx = 0, \end{aligned} \quad (61)$$

since the second term on the left hand side of (60) is non-negative. Note that the two limits in the middle of the above equation are both non-negative. We have

$$\lim_{\alpha \rightarrow \infty} -\frac{1}{\alpha} \int \left(\frac{1}{|x-e_1|} + \frac{1}{|x+e_1|} \right) (|D_{\alpha}\varphi|^2(x-x_+) - |D_{\alpha}\varphi|^2(x-e_1)) dx = 0. \quad (62)$$

This implies that $\min\{|x_+ - e_1|, |x_+ + e_1|\}$ converges to zero, and similarly for x_- . Thus, as $\alpha \rightarrow \infty$, x_{\pm} approaches $\{e_1, -e_1\}$. They cannot converge to the same point, as otherwise the Coulomb interaction is obviously higher. Therefore, we arrive at the conclusion of Theorem 2.

4 Numerical solution to Kohn-Sham SDFT (KS-SDFT) equations for ψ_+ and ψ_- as a function of α

The variation of the energy functional given in Eq. (3) with normalization constraints, leads to Euler-Lagrange equations defining the spin up, ψ_+ , and the spin down, ψ_- , KS-SDFT orbital solutions as a function of exchange strength α and the internuclear bond length, $2R$. In this section we outline the finite element methods (FEM) [9, 14, 35] we used to produce numerical solutions to these equations and

determine their stability. These solutions, characterized by the symmetry of the orbital functions and their localization within the molecular framework, were used to explore the transitions between the regions of stability identified by the theorems in Sections 2 and 3. In the process of generating numerically stable solutions to the Euler Lagrange equations several new classes of solutions were identified. These may have important consequences for the application of Kohn-Sham methods but were not analyzed in Sections 2 and 3. The stability and stationary character of the solutions generated with variation in the R parameter are validated via Hessian analysis (see the Appendix).

An important feature of the FEM approach we used is that the expansions of ψ_- and ψ_+ in the FEM basis [45] are not constrained by any preconceived notion as to the nature of the solution as is implicit in the atomic orbital expansion basis of quantum chemistry software [49, 61, 24]. This is particularly important in our application because of the form of the KS solutions to (3) as a function of α (e.g., for large α) are unknown. The numerical problem and the FEM method we developed for its solution are described in more detail in the Appendix. A novel feature of the numerical method we have used is that its time to solution scales linearly with the size of the basis [35].

4.1 Overview of numerical method (FEM)

Our numerical implementations are based on application of the Python FEniCS finite element (FEM) package [45, 35], which is a collection of free software with an extensive list of features for automated, efficient, finite element solution methods for differential equations. The source codes implementing the linear scaling finite element solver described below can be found at the FEniCS project homepage.² More details specific to our calculation are given in the Appendix.

The FEM calculation domain used here is a fixed square box of dimension $50 \times 50 \times 50$ atomic units which easily contains the H_2 molecule (size ≈ 2 atomic units). Because the bound state molecular orbitals decay exponentially away from the positions of the nucleus, we apply zero boundary conditions at the domain edges for the wave functions. The Coulomb potentials required in the calculation are calculated from Poisson's equation using free space boundary conditions. The singularities of the attractive nuclear potentials, (1) are numerically removed by adding a small positive constant in the denominator [35].

To accommodate the more rapid variation of the ψ functions near the atomic nucleus the finite element grid is adapted within the domain, see Figure 1. This is an essential feature of atomic and molecular electronic structure calculations [16, 38, 17] that do not introduce pseudopotentials [18].

²<https://fenicsproject.org>

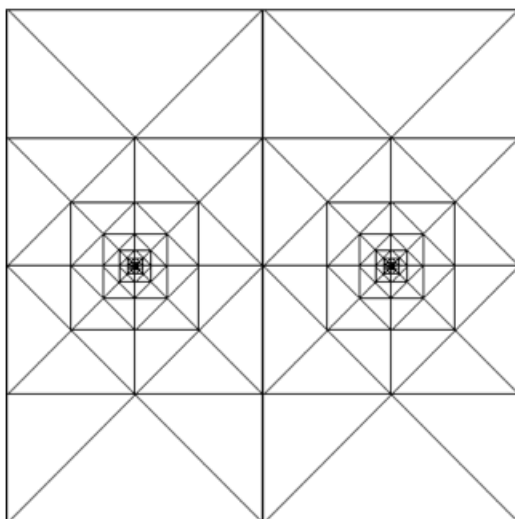


Figure 1: A representation of the finite element grid used in calculation. Each triangle represents a tetrahedron in the real calculation. Note that the density of the mesh is significantly increased near the two atomic nuclei (see Appendix for further discussion as to how this mesh is generated).

In these FEM calculations each molecular orbital (ψ_+ or ψ_-) is written as an expansion in a finite element basis, η_i , with local support centered on the grid points in Figure 1 [45, 16, 9], giving,

$$\psi_{\pm} = \sum_{j=1}^M c_{\pm,j} \eta_j. \quad (63)$$

There are M basis functions, where M is the total number of points in the grid and η_i the finite element basis functions (piecewise linear elements with local support) (see Appendix and [16] for more detail). The variation of the functional (3) expanded in the basis as in (63) leads to generalized eigenvalue problems which must be solved in a self-consistent fashion. These may be written as,

$$\left(-\frac{1}{2}\Delta - \epsilon_{\pm}\right)\psi_{\pm,i}(x) = V_{\text{eff},\pm}[\rho_{\pm}]\psi_{\pm}(x), \quad (64)$$

where the spin electron density is $\rho_{\pm} = |\psi_{\pm}|^2$ and $V_{\text{eff},\pm}[\rho_{\pm}]$ denotes the effective (spin)-potential corresponding to ρ_{\pm} . Only the lowest spin up and spin down states are occupied and only these states are found in the solution method (Appendix), thus we only need the lowest eigenfunction in (64). The eigenvalue problems, (64), are solved using an iterative process in which for step k the ψ_{\pm} on right hand side of (64) and the orbital energies, ϵ_{\pm}^k , at step k are assigned the values and functionality from the $k-1$ step (see Appendix and [35]).

(64) is solved using the FEniCS software package (see Appendix and [35] for more detail). This package implements a conjugate gradient solver (generalized minimal residual method, GMRES [59]) after preconditioning with an algebraic multigrid preconditioner (AMG, BoomerAMG from the Hypre Library [2, 15, 64, 62, 27]). The application of the AMG solver leads to a linear in basis set size to solution time numerical method [35].

Initial guesses for the molecular orbitals (MOs) for the FEM solutions are necessary to start the iteration. Here we used the H atom Slater Type Orbitals (STO-3G) generated from the NWChem data

base [63, 4] to form molecular orbitals for all α . Given two STO-3G functions centered on the atom centers and designated as ϕ_1 and ϕ_2 , the initial unnormalized MOs for symmetric delocalized solutions are $(\phi_1 + \phi_2)/2$. When localized solutions are expected the initial functions are taken to be the STO-3G functions ϕ_1 and ϕ_2 localized on the different atomic centers, see [34, 24].

When α is very small (weak exchange), the final solutions are always the paramagnetic delocalized states that converge to the same spatial dependence for spin up and spin down states (i.e., $\psi_+ = \psi_-$, where these are the lowest energy solutions for each spin). For very large α the lowest energy states may be strongly localized (i.e., the spin up and spin down single electron states are localized on different atomic centers). These localized solutions may not be well approximated by the STO-3G initial functions. However, we have not had problems with convergence of the method used and described in the Appendix.

In summary, in our FEM formalism the forms of the spatial parts of the orbital wave functions are completely independent and the symmetry of the total density is not constrained. However, for most of the stationary solutions that we have found the total electron density retains the symmetry of the H_2 molecule. We have shown above this to be true for the ρ calculated from the lowest energy solutions of (3) in both the large α and small α limits. However, for the lowest energy product state the symmetry of the spatial parts of the individual spin orbitals may be broken in a way that preserves the symmetry of the total density of the molecule leading to localization of the electron spin. Additional higher energy numerical solutions have been identified which do not preserve the symmetry of the molecule (see Figure 4). In applications of DFT to large molecules or condensed materials this spin localization is interpreted in terms of the observed spin states of lattices (or molecules) (e.g. antiferromagnetic states in condensed materials [22, 56, 51]).

4.1.1 Bifurcation in the R dimension

The optimized total energy as the H_2 molecular bond, $2R$, is lengthened at fixed $\alpha = 0.93$ (see (3) similar to the value used in the application of SDFT to molecular and condensed matter problems) is shown in Figure 2. The accuracies of the total energies calculated are within 0.02 au for the H_2 molecule in our calculations reported here, see [35]. Remarkably, for a given α and sufficiently small R , the independent solutions for orbital wave functions ψ_+ and ψ_- converge to the same function even under full variation with no symmetry restriction. (That is to say, there is NO symmetry breaking in the molecular orbitals.) This is consistent with the fixed R , small α analysis in Section 2. In this region, the *restricted* DFT (RDFT) solution in which ψ_+ and ψ_- are taken to be the same function (double filling) is the lowest energy solution to the optimization problem posed in (3) even when each orbital function is varied independently without constraint. Similar behavior is observed in the Hartree or Hartree-Fock model of electronic structure for the two electron system. These solutions are important because such doubly filled restricted DFT solutions are widely assumed and used in quantum chemistry applications [24, 61].

As the H_2 bond length is extended as illustrated in Figure 2 ($2R \gtrsim 2.45\text{au}$) the solution bifurcates creating two two-electron product (singlet determinant [61, 50]) solutions. In the lowest energy state (lower branch, green line) one symmetry broken electron orbital (say the spin up state) is localized around one site and the other orbital function state (spin down) is localized around the second nuclear site (see the green density distribution cartoon in the bottom right Figure 2). The product wave function (total density) for this branch leads to a spin localized density distribution (*spin up and spin down electrons localized on different atomic sites with total spin zero and preserving the symmetry of the molecule*). This spin distribution is consistent with an antiferromagnetic state for the H_2 molecule. Since spin ordered condensed systems are common targets for DFT prediction, this is an important dimension for variation in designing DFT representations of such systems [22, 56, 51].

The upper energy branch in Figure 2 is a continuation of the restricted solution in which the spin

up and spin down orbitals have the same spatial dependence (no localization, blue density distribution bottom right Figure 2). We note that this solution continues as a stationary solution even for large R . To better illustrate the structure of the solution as R goes from the restricted region to the antiferromagnetic region we plot the spin-up density weight of ψ_+ defined as

$$w_+ = \int_{x_1 \geq 0} |\psi_+(x)|^2 dx, \quad (65)$$

where the integration is on the right half domain corresponding to regions closer to one of the nuclei. This is the proportion of the mass of ψ_+ localized near one of the nuclei (and $w_+ = 1/2$ if no localization happens). Here we have identified ψ_+ as the spin function which after the bifurcation is more localized in the positive x_1 region. We note the smooth behavior of the variation of w_+ as the bond length enters the bifurcated region, observed in Figure 3. The plot further confirms the symmetry bifurcation as R increases. Note that the symmetry of total electron density is preserved in both the upper and lower states as in insert in Figure 2.

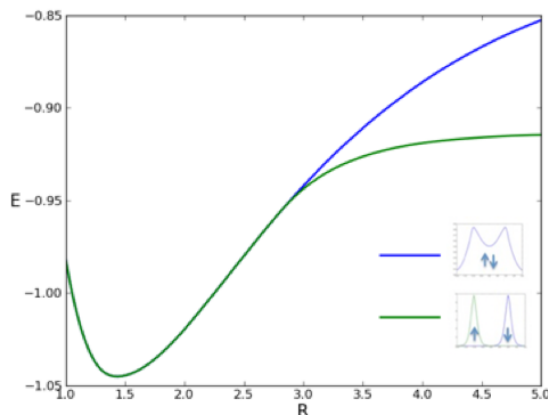


Figure 2: Bifurcation of LSDA for H_2 in the R dimension with $\alpha = 0.93$. The bifurcation point is in the region $2R = 2.40$ to 2.50 au. The energy difference between the two states in the region $2R = 2.40$ to 2.50 au is of the order of 10^{-5} au.

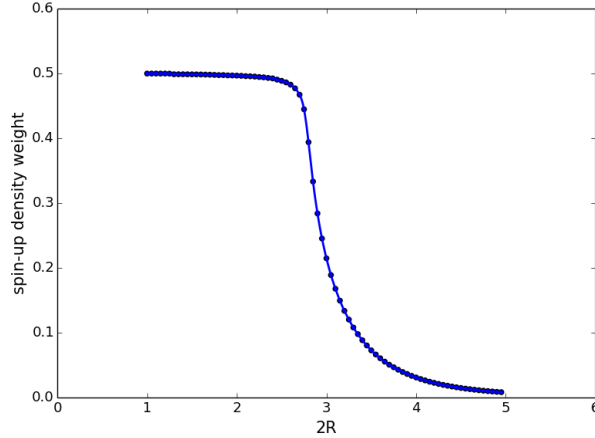


Figure 3: Spin-up density weight, w_+ (defined in (65)) as a function of bond length

4.1.2 Hessian of bifurcated solutions for R variation

After the bifurcation with increasing R , Figure 2, there are two antisymmetric solutions to the electron mean field problem (one spin localized/antiferromagnetic (green line) and one restricted (no localized spin, blue line)). This is similar to the application of DFT methods to real systems (e.g., magnetic materials) in which several solutions (spin orderings) may be found as stationary [18, 56, 51]. These states are frequently interpreted in terms of the relative spin ordering of phases of different structure with apparent reliability. These calculation produce results which correlate well with experimental observations in [18, 56, 51]. However, in a realistically sized calculation it can be difficult to identify the minimum energy structure on the basis of currently used optimization methods [18, 56]. (For a brief overview of how spin is controlled in condensed matter calculations, see reference [18].)

The stability/metastability of the solutions to the H_2 problem along the 2 branches In Figure (2) can be determined by analyzing the eigenvalues of the Hessian associated with the optimization problem (3) (see the Appendix). For stationary solutions the gradient of the total energy (constrained to have the proper normalization) must be zero for any dissent direction. For stable stationary solutions all eigenvalues of the Hessian (see the Appendix) must be positive. If a solution is unstable there will be at least one negative eigenvalue of the Hessian. At the bifurcation point, there will be a zero eigenvalue.

Numerical estimates of the eigenvalues of the Hessian the optimization problem (3) (also calculated via the FEM see appendix) are reported in Table 1. These show there is one negative eigenvalue for the delocalized RDFT solution (green line Figure 2) beyond the bifurcation point. The combination of the zero gradient and the presence of the single negative eigenvalue shows that this is a metastable point in the energy surface.

Bond Length	Solution	Result	Details
2.0 a.u.	delocalized	Local Minimizer	all eigenvalues on the constraint manifold > 0 .
3.5+ a.u.	delocalized	Saddle Point	1 eigenvalue on the constraint manifold < 0 .
3.5+ a.u.	localized	Local Minimizer	all eigenvalues on the constraint manifold > 0 .

Table 1: Eigenvalues for the Hessian matrix, $\alpha = 0.93$ for various bond lengths

4.1.3 Bifurcation in the α dimension

We demonstrate here the numerical verification of the results in Theorems 1 and 2. Adjustment of parameters such as the strength of exchange, α , in (3) in the density functional formalism is sometimes used to improve DFT model performance for spin ordered systems [52, 56]. In the H_2 problem discussed here the parameters $2R$ and α control the bifurcation. For a given R the strength of the exchange term determines the bifurcation point. Figure 4 shows the symmetry breaking bifurcation points for LSDA solutions of (3) with strength of the exchange contribution for fixed bond lengths $2R = 2.0\text{au}$.

In the small α setting, there are two identical degenerate spatial solutions (for spin up and spin down). These solutions (delocalized solutions) have peaks at the two atom centers, spread over the whole molecule and have the symmetry of the molecule. In this region, if numerical solutions are initiated with broken symmetry the ψ_+ and ψ_- solutions evolve to have the same spatial dependence, i.e., $\psi_+ = \psi_-$. These solution are equivalent to the single orbital solution of the restricted or doubly filled DFT product function.

See the analysis in Section 2 for the demonstration of this result, but the underlying reason is that the Coulomb repulsion is somewhat insensitive to the localization of the total density and the kinetic energy dominates over the exchange potential contribution in (3). Beyond the bifurcation point (as illustrated in Figure 2, the broken symmetry solutions with excess spin concentrate on each atom (localized solutions) appears and the product solution with equivalent spin localization on each site is the global minimizer. The total density still has the symmetry of the molecule. The restricted solutions with higher energy are still stationary along the upper branch of the bifurcation curve. These solutions have not been discussed in our analysis.

As α is further increased (at constant R) a variety of new bifurcations appear. The exchange potential contributes much more than the Coulomb potential so the solution tends to be localized instead of delocalized. We note that the antiferromagnetic solution (blue line) is the global solution for all large α . This is an important result since this is the solution generally associated with magnetic behavior in real materials. The symmetric delocalized solution (dark green and light green lines in Figure 4) is the highest energy. For very high α the maximum density moves to the middle of the bond. For $\alpha > 6$ the high energy delocalized solutions break symmetry and forms two stable lower energy two electron solutions centered on the atom centers (red line in Figure 4).

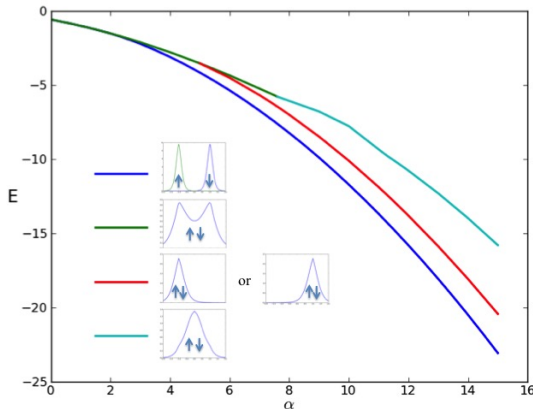


Figure 4: Several numerically constructed branches of the bifurcation of LSDA for H_2 in the α parameter with $R = 2.0\text{au}$ showing the relevant ψ_{\pm} profiles.

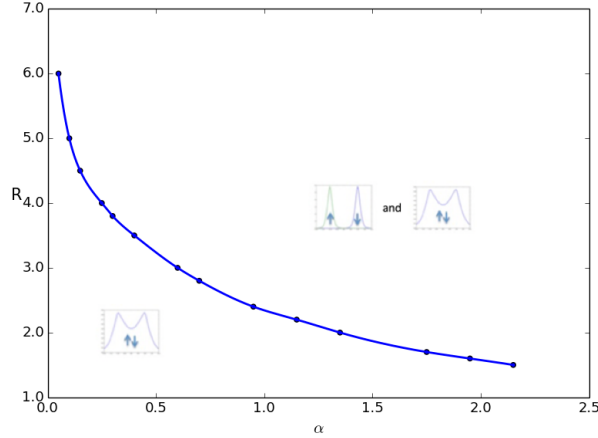


Figure 5: The first symmetry breaking bifurcation of LSDA for H_2 as a phase diagram in R and α . Below the line only delocalized states are present while above the line there are both delocalized and localized states.

For applications to real materials the bifurcation in R for a fixed α is taken as the onset of magnetic behavior. The bond length corresponding to beginning of antiferromagnetic behavior (spin localization) occurs after the first bifurcation. In Figure 5 we show the variation of the first R bifurcation point for different α . For α in the region commonly used the bond length for bifurcation is quite sensitive to the strength of exchange.

5 Discussion and future works

A similar analysis to the large α case gives that the ground state Euler-Lagrange equation for large R can be transformed to an equation of the form

$$-\Delta\psi_{\pm}(x) + R^2 E(R)\psi_{\pm}(x) - RV_1(x)\psi_{\pm}(x) + R \int \frac{|\psi_+|^2(y) + |\psi_-|^2(y)}{|x-y|} dy \psi_{\pm}(x) + R\alpha|\psi_{\pm}(x)|^{\frac{2}{3}}\psi_{\pm}(x) = 0, \quad (66)$$

taking $\psi_{\pm}(x) = R^{\frac{3}{2}}\psi_{\pm}(Rx)$. For $R \gg 1$, this is related to a new problem with large Coulomb repulsion, large but unit distance apart nuclear masses $Z = R$, and a strong exchange-correlation nonlinearity $R\alpha$. Thus, the main issue is to study the nature of the stable curve for a large nuclear mass with strong exchange-correlation nonlinearity and observe what the nature of the Lagrange multiplier $R^2 E(R)$ should be as $R \rightarrow \infty$. The intuition is that this scales the problem to be localized since moving along the stable branch of states from low electron mass (small Lagrange multiplier) for the potential V_1 to large electron mass (large Lagrange multiplier) eventually concentrates onto localized states over each well. This suggests that we consider a modified Lagrangian with critical points given by

$$-\epsilon^2 \Delta\psi_{\pm}(x) + \psi_{\pm} - V_1\psi_{\pm} + \int \frac{|\psi_+|^2(y) + |\psi_-|^2(y)}{|x-y|} dy \psi_{\pm}(x) + \alpha|\psi_{\pm}(x)|^{\frac{2}{3}}\psi_{\pm}(x) = 0, \quad (67)$$

where the small parameter $\epsilon = 1/\sqrt{R}$. This looks like a Ginzburg-Landau type singular-perturbation. As a result, this motivates the following question for a (strange) Hydrogen model (it is strange since a Coulomb self-repulsion and an exchange energy for a single electron are included): Is the minimizer of

$$E_H(u) = \frac{1}{2} \int |\nabla u|^2 dx - \int \frac{Z}{|x|} |u|^2(x) dx + \frac{1}{2} \iint \frac{|u|^2(x)|u|^2(y)}{|x-y|} dx dy - \int |u|^{8/3} dx \quad (68)$$

such that $\|u\|_{L^2} = 1$ orbitally stable. This has been answered in some sense when $Z = 0$ in [57] when the mass is that of the absolute minimizer. Understanding what occurs for the natural electronic mass 1 requires further investigation of this model and will be a topic of future work.

Acknowledgements

We thank the anonymous referee for a very careful reading of this work and making many useful suggestions both to improve the exposition and clarify several points in the analysis. The work of J.L. is partially supported by the National Science Foundation under grants DMS-1312659 and DMS-1454939 and by the Alfred P. Sloan Foundation. J.L.M. was supported in part by NSF Applied Math Grant DMS-1312874 and NSF CAREER Grant DMS-1352353.

A Appendix

We recall here the basics of the finite element methods we use in this work to numerically find the critical points of the XLDA Lagrangian. The numerical algorithms are implemented using a *python* implementation of the FENICS finite element package, [23]. Many of the tools we use here are discussed in more detail in the references [16, 35]. For complete discussions of Finite Element Methods, see the books of [5, 6, 9, 14]. The method we develop here takes advantage of the sparsity of the FEM representation of the eigenvalue problem leading to an algorithm that scales linearly with number of basis functions. For resources on large scale computing in computational chemistry, see [36, 63].

I. The Finite Element Set Up

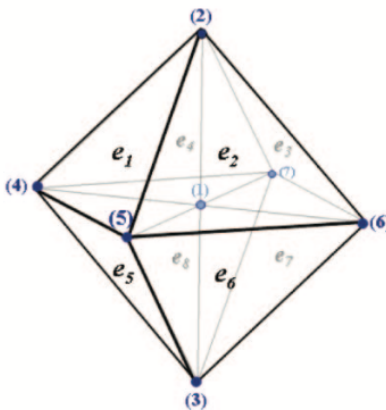


Figure 6: Finite element tetrahedron defining FEM elements and nodes. The L tetrahedral elements are identified by e_l . The global nodes are indexed by (m) . For each element e_l there is a global node at each corner. Generally local nodes belonging to individual tetrahedra are also defined. See [14, 5, 9, 16]. These are not shown and are managed transparently by the Dolfin software [46].

We assume that the solution, ψ_{\pm} exists in a bounded domain $\Omega \in \mathcal{R}^3$ that can be divided into a set of L non overlapping tetrahedral elements, $\{e_l\}_{l=1}^L$ [14, 5, 9, 16], see Figures 6 and 1. For the electronic structure problems we are concerned with the atomic potentials represented by $V(x)$ in the Hamiltonian below, (74), are singular. This leads to rapid variation of the solution to the eigenvalue problem in this

region. In order to obtain accuracy the FEM grid in this region must have a finer resolution as illustrated in Figure 1 and discussed in [17, 38, 16].

To construct the grid used in the calculation, we:

1. Use BoxMesh [45] to generate a coarse mesh in a $50 \times 50 \times 50$ domain. The initial number of cells in each direction is 2. So the total number of tetrahedra will be 48 and the total number of vertices will be 27 in the coarse mesh.

2. Find the closest mesh grids to the nuclei and set the parameter *cell_marker* [45] true that tells the code to refine the mesh. If *cell_marker* = false, it means this mesh will NOT be refined.

3. Refine the whole grid for 3 cycles.

Generally FEM nodes are located at corners, along boundaries or in the centers of tetrahedral regions [14, 5, 9, 1]. For the calculations here the nodes are located only at the corners of the tetrahedra. These nodes are shared by adjacent tetrahedra as in Figure 6. Each tetrahedron l has four corner nodes. A global index identifies a node as in Figure 6 (global node numbers in brackets). There are M global nodes in the construction. In actual calculations a local node index identifying a corner global node with a basis function inside a particular tetrahedral is also defined in Dolfin [1, 5, 9, 14, 16] to identify variation associated with a node within a particular tetrahedron [1, 5, 9, 14]. The somewhat difficult book keeping problem of keeping track of the global variation of the basis functions consistent with their local behavior is taken care of nicely in the FEniCS software, see [45].

For each node (with global index m and local index i) in a tetrahedral element, l , a finite element basis functions $\{\chi_i^{e_l}\}$ is defined. In these calculations the $\{\chi_i^{e_l}\}$ are linear functions centered on local nodes i in element e_l [1, 16, 14, 5, 9]. For each global node m the linear basis function $\{\chi_i^{e_l}\}$ is 1 on global node i and zero on all other nodes contained in the tetrahedral elements containing global node m . For a particular tetrahedron the linear basis associated with local node i of tetrahedral e_l , $\{\chi_i^{e_l}\}$, has value only in tetrahedra e_l . Illustrations of how this works are given in [1]. The local node functions $\{\chi_i^{e_l}\}$ can be assembled in functions centered around the global nodes with index m as the global basis functions $\eta_m(x)$.

A piecewise continuous function (here the approximated $\psi_{\pm}(x)$) can now be expanded as in [16],

$$\psi_{\pm}(x) = \sum_{m=1}^M c_{\pm,m} \eta_m(x). \quad (69)$$

Here, M is the dimension of space of global nodes and $c_{\pm,m}$ is the coefficient of basis element η_m . The value of the ψ_{\pm} on node m is $c_{\pm,m}$.

II. The Generalized Eigenvalue Problem:

With the above formulation, solving the Kohn-Sham minimization problem related to (3) leads to the generalized eigenvalue problem (in many of the following equations the \pm (+ spin up, – spin down) notation has been suppressed to keep notation simple),

$$\mathbf{Hc} = \epsilon \mathbf{Sc}, \quad (70)$$

or

$$\sum_n H_{mn} c_{n,k} = \epsilon_k \sum_n S_{mn} c_{n,k} \quad (71)$$

where k identifies the k^{th} eigenfunction,

$$S_{mn} = \int_{\Omega} dx \eta_m(x) \eta_n(x), \quad (72)$$

and

$$H_{mn} = \frac{1}{2} \int_{\Omega} dx \nabla \eta_m(x) \nabla \eta_n(x) + \int_{\Omega} dx \eta_m(x) V_{\text{eff}} \eta_n(x) \quad (73)$$

with V_{eff} given by

$$V_{\text{eff}} = V_{\text{ext}}(x) + V_{\text{ee}}(\rho) + V_{\text{ex}}(\rho, \alpha) = V_{\text{ext}}(x) + \int \frac{\rho(x')}{|x-x'|} dx' + V_{\text{ex}}(\rho_{\pm}, \alpha). \quad (74)$$

Here $\rho(x)$ is the total electron density, and ρ_{\pm} is the spin density, and $V_{\text{ex},\pm}(\rho_{\pm}, \alpha)$ is given by the scaled Dirac form

$$V_{\text{ex},\pm}(\rho, \alpha) = \alpha \rho_{\pm}^{1/3}. \quad (75)$$

Note that in the spin DFT, the exchange potential depends on the spin component, and thus the effective Hamiltonian for the spin-up and spin-down orbitals are different; while the structure of the problem is the same, and hence we keep the notation (e.g., for \mathbf{H} and \mathbf{S}) independent of spin component. The matrix H_{mn} , (73), the overlap matrix S_{mn} , (72) and integrals over $V(x)$ in (74) can be obtained from the FEniCS software [45]. The calculation of these matrix are also carefully discussed for the electronic structure problem in [16] and in general in [14, 5, 9]. The full potential V_{eff} given by (74) is a function of the density requiring that the eigenvalue problem, (70), be solved iteratively until self consistency is achieved. We are only interested in the lowest \pm energy solutions, though the methods can be modified to higher energy states as well.

III. Solution to the generalized eigenvalue problem and the associate Coulomb problem

The objective of the calculation is the solution of the generalized eigenvalue problem, (70). However, this requires the input of a current estimate of the Classical potential V_{ee} required in V_{eff} , (74). This may be found as the solution to the Poisson equation

$$\Delta V_{\text{ee}} = -4\pi \rho = -4\pi \left[|\psi_+|^2 + |\psi_-|^2 \right] \quad (76)$$

To solve this PDE V_{ee} is also expanded in the finite element basis as,

$$V_{\text{ee}}(x) = \sum_{m=1}^M v_m \eta_m(x). \quad (77)$$

(76) is then represented by a system of linear equations giving the $\{v_m\}$. Given a solution to the Coulomb problem, (76), based on a current density for the iteration, the generalized eigenvalue problem, (70) is also solved in the $\{\eta_m\}_{m=1}^M$ finite element basis functions. Each molecular orbital is represented as

$$\psi_{\pm} = \sum_{\alpha=1}^M c_{\pm, \alpha} \eta_{\alpha}. \quad (78)$$

Note, for this problem there is only one filled molecular orbital for each spin. The finite element discretization of the one-electron equation for the current iteration is given as, for $i = \pm$

$$(T_i - \epsilon_i) c_i = v_i. \quad (79)$$

$c_i = \{c_{i1}, \dots, c_{im}\}$ are the coefficients of molecular orbital in the expansions of finite element basis. The elements of the operator $(T_i - \epsilon_i)$, are,

$$(T_i - \epsilon_i)_{mn} = \int_{\Omega} \left\{ \frac{1}{2} \nabla \eta_m \nabla \eta_n - \epsilon_i \eta_m \eta_n \right\} dx. \quad (80)$$

The elements of v_i are given by

$$(v_i)_m = \int \eta_m(x) V_{\text{eff},i}(x) \psi_i(x) dx \quad (81)$$

are calculated in an iterative process in which $V_{\text{eff},i}(x)$ is defined for step k from the results of the self-consistent solver in the prior iteration.

Details of the FEniCS solver

The AMG solver is based on a V-cycle [15, 35] with a maximum number of multi grid levels of 25. For each fine to course grid transfer a single pre smoothing step is taken. For each course to fine transfer a single post smoothing step is taken. These smoothing steps use a symmetric-SOR/Jacobi method. On the coarsest level the course FEM equation is relaxed by Gaussian elimination. In the iteration an energy correction step is applied to update new eigenvalues after the Helmholtz equation is solved for a set of $\epsilon^{(k)}$ from the prior AMGCG cycle. The self-consistent solver converges when the total energy difference in two consecutive iterations is smaller than a selected tolerance. These are solved via the FEniCs code using the GMRES [59] and BOOMER AMG (Algebraic Multigrid [15]) packages. The solution to this problem is of order M [35]. To improve the convergence of the solution a preconditioning based on the algebraic multigrid method is used [62, 64]. For an introduction to multigrid methods and their application to problems in electronic structure, see [17, 38, 15, 10, 11, 12, 13, 32, 33, 47].

IV. The Wavefunction and Orbital Energy update and iteration

IV.i: Some Preliminaries

The eigenvalue problem, (79), is solved using an iterative process in which for step k the ψ_{\pm} on right hand side of (79) and the orbital energies, $\epsilon_{\pm}^{(k)}$, at step k are assigned the values and functionality from the $k-1$ step. The iteration is developed with the intention of producing linear scaling in the number of FEM basis functions, M . This is achieved by developing a solver strategy that emphasizes the use of the operator $[(\nabla^2 - k^2)]^{-1}$ which is efficiently implemented in multigrid schemes.

The density functional equations leading to the values of ϵ_i^k and ψ_i^k for the k values (update from $\psi_i^{(k-1)}$ to ψ_i^k) are written as

$$\left[-\frac{1}{2} \nabla_x^2 - \epsilon_i^{(k-1)} \right] \psi_i^k(x) = \left[V_{\text{ext}}^{(k-1)}(x) + V_{\text{ee}}^{(k-1)}(\rho^{(k-1)}(x)) + V_{\text{ex}}^{(k-1)}(\rho^{(k-1)}(x)) \right] \psi_i^{(k-1)}(x) \quad (82)$$

where V_{ext} is the external potential from (1). The electron-electron Coulomb potential (calculated from FeniCS as above) is given by,

$$\nabla^2 V_{\text{ee}}^{(k-1)}(x) = -4\pi \rho^{(k-1)}(x) = -4\pi \left[\left| \psi_+^{(k-1)} \right|^2 + \left| \psi_-^{(k-1)} \right|^2 \right]. \quad (83)$$

The exchange potential is given by,

$$V_{\text{ex}}^{(k-1)}(x) = \alpha \rho^{(k-1)}(x)^{\frac{1}{3}}. \quad (84)$$

This is now a linear PDE of the form,

$$\left[-\frac{1}{2} \nabla^2 - \epsilon_i^{(k-1)} \right] \psi_i^k(x) = f_i^{(k-1)}(x). \quad (85)$$

Note that all the potential terms in (82) have been collected in the function $f_i^{(k-1)}$. We calculate the solution to (85) using an efficient multigrid method. Because of the complexity of the grid we use the AMGCG implemented in the FEniCS software [45].

IV.ii: Update of the wavefunction, from $\psi^{(k-1)}(x)$ to $\psi^k(x)$:

To initiate the k^{th} iteration ($\psi_i^{(k-1)}$ to ψ_i^k) we assume we have solutions $\psi_i^{(k-1)}(x)$ and $\epsilon_i^{(k-1)}$. The update of the wavefunction proceeds directly from (85) as

$$\psi_i^k(x) = \left[-\frac{1}{2}\nabla_x^2 - \epsilon_i^{(k-1)} \right]^{-1} f_i^{(k-1)}(x). \quad (86)$$

All the functions in this equation are defined from the solution that we obtain from AMGCG.

To complete the iteration cycle we also need an update of the orbital energy $\epsilon_i^{(k-1)}$ to ϵ_i^k .

IV.iii: Update of the orbital energy:

We assume we have $\psi_i^{(k-1)}(x)$ and $\epsilon_i^{(k-1)}$. and begin by defining two Greens functions:

The $(k-1)^{\text{th}}$ Green's function, $G_i^{(k-1)}$, with energy $\epsilon^{(k-1)}$,

$$G_i^{(k-1)} = \left\{ -\frac{1}{2}\nabla^2 - \epsilon_i^{(k-1)} \right\}^{-1} \quad (87)$$

and a Green's function, G_i^{con} with the converged DFT orbital energy (from converged solution to DFT equations), ϵ_i^{con} . This is given by,

$$G_i^{\text{con}} = \left\{ -\frac{1}{2}\nabla^2 - \epsilon_i^{\text{con}} \right\}^{-1}. \quad (88)$$

In the iteration, the updated ϵ_i^k , given by

$$\epsilon_i^k = \epsilon_i^{(k-1)} + \delta\epsilon_i^k. \quad (89)$$

is taken to be a good approximation to ϵ^{con} . Using this in (88) we have,

$$G_i^{\text{con}} = \left\{ -\frac{1}{2}\nabla^2 - \epsilon_i^{\text{con}} \right\}^{-1} = \left\{ \frac{1}{2}\nabla^2 - (\epsilon_i^{(k-1)} + \delta\epsilon_i^k) \right\}^{-1} \quad (90)$$

the objective is to calculate an orbital energy correction from these equations using $\psi_i^{(k-1)}$.

The function ψ_i^{con} satisfies the orbital PDE,

$$\psi_i^{\text{con}}(x) = \left\{ -\frac{1}{2}\nabla^2 - \epsilon_i^{\text{con}} \right\}^{-1} f_i^{\text{con}}(x). \quad (91)$$

In this equation ϵ_i^{con} is the converged orbital energy.

We assume that $\psi_i^{(k-1)}$ is a good approximation to ψ_i^{con} , i.e., that it approximately satisfies

$$\psi_i^{(k-1)}(x) = \left\{ -\frac{1}{2}\nabla^2 - \epsilon_i^{\text{con}} \right\}^{-1} f_i^{(k-1)}(x) = \left\{ -\frac{1}{2}\nabla^2 - (\epsilon_i^{(k-1)} + \delta\epsilon_i^k) \right\}^{-1} f_i^{(k-1)}(x). \quad (92)$$

Now we expand the full Green's function (RHS) in the energy correction $\delta\epsilon_i^k$ to obtain an equation that will update the orbital energy (find a correction to $\epsilon_i^{(k-1)}$).

We use the operator identity,

$$\frac{1}{(1+a+b)} = \frac{1}{(1+a)} + \frac{1}{(1+a)} \frac{-b}{(1+a+b)}, \quad (93)$$

to obtain

$$\left\{ -\frac{1}{2}\nabla^2 - \epsilon_i^{(k-1)} - \delta\epsilon_i^k \right\}^{-1} = \left\{ -\frac{1}{2}\nabla^2 - \epsilon_i^{(k-1)} \right\}^{-1} - \left[\left\{ -\frac{1}{2}\nabla^2 - \epsilon_i^{(k-1)} \right\}^{-1} \right. \\ \left. \left\{ -\delta\epsilon_i^k \right\} \left\{ -\frac{1}{2}\nabla^2 - \epsilon_i^{(k-1)} - \delta\epsilon_i^k \right\}^{-1} \right]. \quad (94)$$

Iteration of this equation leads to an expression for the propagator to 1st order in $\delta\epsilon_i^k$ as,

$$\left\{ -\frac{1}{2}\nabla^2 - \epsilon_i^{(k-1)} - \delta\epsilon_i^k \right\}^{-1} = \left\{ -\frac{1}{2}\nabla^2 - \epsilon_i^{(k-1)} \right\}^{-1} - \left[\left\{ -\frac{1}{2}\nabla^2 - \epsilon_i^{(k-1)} \right\}^{-1} \right. \\ \left. \times \left\{ \delta\epsilon_i^k \right\} \left\{ -\frac{1}{2}\nabla^2 - \epsilon_i^{(k-1)} \right\}^{-1} \right]. \quad (95)$$

We can use this result in (92) to give,

$$\psi_i^{(k-1)}(x) = \left\{ -\frac{1}{2}\nabla^2 - \epsilon_i^{(k-1)} \right\}^{-1} f_i^{(k-1)}(x) \\ - \left\{ -\frac{1}{2}\nabla^2 - \epsilon_i^{(k-1)} \right\}^{-1} \delta\epsilon_i^k \left\{ -\frac{1}{2}\nabla^2 - \epsilon_i^{(k-1)} \right\}^{-1} f_i^{(k-1)}(x). \quad (96)$$

This is more conveniently written in vector notation [21] as,

$$\left| \psi_i^{(k-1)} \right\rangle = \left\{ -\frac{1}{2}\nabla^2 - \epsilon_i^{(k-1)} \right\}^{-1} \left| f_i^{(k-1)} \right\rangle \\ - \left\{ -\frac{1}{2}\nabla^2 - \epsilon_i^{(k-1)} \right\}^{-1} \delta\epsilon_i^k \left\{ -\frac{1}{2}\nabla^2 - \epsilon_i^{(k-1)} \right\}^{-1} \left| f_i^{(k-1)} \right\rangle \quad (97)$$

or

$$0 = - \left| \psi_i^{(k-1)} \right\rangle + \left\{ -\frac{1}{2}\nabla^2 - \epsilon_i^{(k-1)} \right\}^{-1} \left| f_i^{(k-1)} \right\rangle \\ - \left\{ -\frac{1}{2}\nabla^2 - \epsilon_i^{(k-1)} \right\}^{-1} \delta\epsilon_i^k \left\{ -\frac{1}{2}\nabla^2 - \epsilon_i^{(k-1)} \right\}^{-1} \left| f_i^{(k-1)} \right\rangle. \quad (98)$$

Closing this equation on the left with $\langle f_i^{(k-1)} |$ gives a linear expression for $\delta\epsilon_i^k$ which may be in terms of the ψ_i^k , (86) , as,

$$0 = - \langle f_i^{(k-1)} | \psi_i^{(k-1)} \rangle + \langle f_i^{(k-1)} | \psi_i^k \rangle \\ - \delta\epsilon_i^k \langle \psi_i^k | \psi_i^k \rangle. \quad (99)$$

This may be solved for $\delta\epsilon_i^k$ to obtain

$$\delta\epsilon_i^k = \frac{- \langle f_i^{(k-1)} | \psi_i^{(k-1)} \rangle + \langle f_i^{(k-1)} | \psi_i^k \rangle}{\langle \psi_i^k | \psi_i^k \rangle}. \quad (100)$$

This gives the update to $\epsilon_i^{(k-1)}$ via (89) to complete the k^{th} iteration.

V. The Self Consistent Iteration

Algorithm 1 summarizes the process followed by the self-consistent solver. An initial guess (c_i^0, ϵ_i^0) , $i = 1, \dots, n$ is given to start the self-consistent iterations. The solver stops when the total energy difference in two consecutive iterations is smaller than the tolerance TOL.

Algorithm 1 The Self-consistent Iteration

Input (c_i^0, ϵ_i^0) , $i = 1, \dots, n$, TOL;
while $\|\epsilon_{\text{total}}^k - \epsilon_{\text{total}}^{(k-1)}\| > \text{TOL}$ **do**
 Evaluate potentials V_{ij}^k , $i, j = 1, \dots, n$;
 Evaluate v_i^k , $i = 1, \dots, n$;
 Solve the Helmholtz equation, and get updated $\{c_i^{(k+1)}, i = 1, \dots, n\}$;
 energy correction step, and get updated $\{\epsilon_i^{(k+1)}, i = 1, \dots, n\}$;
 $k++$;
Output (c_i, ϵ_i) , $i = 1, \dots, n$.

VI. Hessian analysis

The model we investigate in this work is the local spin density approximation (LDA) (without correlation energy contributions). As above the ground singlet state spin unrestricted density functional theory for this two-electron system defines two orbital wave-functions (ψ_+, ψ_-) . The total energy functional is $E(\psi)$ is

$$E_\alpha(\psi_+, \psi_-) = \frac{1}{2} \int |\nabla \psi_+|^2 dx + \frac{1}{2} \int |\nabla \psi_-|^2 dx + \int V_R(x) (|\psi_+(x)|^2 + |\psi_-(x)|^2) dx \\ + \frac{1}{2} \iint \frac{(|\psi_+(x)|^2 + |\psi_-(x)|^2)(|\psi_+(y)|^2 + |\psi_-(y)|^2)}{|x-y|} dx dy - \alpha \int (|\psi_+(x)|^{8/3} + |\psi_-(x)|^{8/3}) dx, \quad (101)$$

where $V_R(x)$ is the nuclear potential. The constraints on (ψ_+, ψ_-) are

$$\int |\psi_i(x)|^2 dx = 1, i = +, -. \quad (102)$$

We define the Lagrangian as,

$$L(\psi_+, \psi_-, \epsilon_+, \epsilon_-) = \frac{1}{2} \int |\nabla \psi_+|^2 dx + \frac{1}{2} \int |\nabla \psi_-|^2 dx + \int V_R(x) (|\psi_+(x)|^2 + |\psi_-(x)|^2) dx \\ + \frac{1}{2} \iint \frac{(|\psi_+(x)|^2 + |\psi_-(x)|^2)(|\psi_+(y)|^2 + |\psi_-(y)|^2)}{|x-y|} dx dy - \alpha \int (|\psi_+(x)|^{8/3} + |\psi_-(x)|^{8/3}) dx \\ - \epsilon_+ \left(\int |\psi_+(x)|^2 dx - 1 \right) - \epsilon_- \left(\int |\psi_-(x)|^2 dx - 1 \right), \quad (103)$$

where (ϵ_+, ϵ_-) are Lagrange multipliers.

Finding the stationary variation of (103) with respect to the functions ψ_+ and ψ_- leads to effective one-electron eigenvalue equations.

$$\frac{\delta L}{\delta \psi_i} = 0 \Rightarrow \left(-\frac{1}{2} \nabla^2 + V_R(x) + \int \frac{(|\psi_+(y)|^2 + |\psi_-(y)|^2)}{|x-y|} dy - \frac{4}{3} \alpha |\psi_i(x)|^{2/3} \right) \psi_i(x) = \epsilon_i \psi_i(x), i = \pm, \quad (104)$$

where (ψ_+, ψ_-) and (ϵ_+, ϵ_-) satisfy normalization constraints.

In order to determine whether the stationary extremum of $L(\psi_+, \psi_-, \epsilon_+, \epsilon_-)$ with respect to functional variation are a maximum, a minimum or a saddle point, the second order functional derivative (the Hessian matrix) may be analyzed [35]. In the following the stationary solutions (ψ_+, ψ_-) and their eigenvalues (ϵ_+, ϵ_-) satisfy (104) and (102). (λ_i, w_i) are eigenvalues and eigenvectors of the Hessian Matrix, **Hess**, defined as the solutions to the eigenvalue problem,

$$\mathbf{Hess} w_i(y) = \int \frac{\delta^2 L(\psi, \epsilon)}{\delta \psi_i(x) \delta \psi_j(y)} w_i(y) dy \Big|_{(\psi, \epsilon) = (\phi, \epsilon)} = \lambda_i w_i(x), \quad i = \pm, \quad (105)$$

where the Hessian matrix is defined as,

$$\mathbf{Hess} = \begin{pmatrix} H_{11} & \int \frac{2\psi_-(y)}{|x-y|} dy \psi_+(x) \\ \int \frac{2\psi_+(y)}{|x-y|} dy \psi_-(x) & H_{22} \end{pmatrix} \quad (106)$$

where

$$H_{11} = -\frac{1}{2}\nabla^2 + V_R + \int \frac{|\psi_-(y)|^2}{|x-y|} dy - \frac{20}{9}\alpha |\psi_+(x)|^{2/3} - \epsilon_+,$$

$$H_{22} = -\frac{1}{2}\nabla^2 + V_R + \int \frac{|\psi_+(y)|^2}{|x-y|} dy - \frac{20}{9}\alpha (|\psi_-(x)|^{2/3} - \epsilon_-).$$

In addition the eigenfunctions $w_i(x)$ satisfy the orthogonality relations,

$$\int \psi_i(x) w_i(x) dx = 0, \quad i = +, -. \quad (107)$$

If all the eigenvalues of **Hess** are positive, then there is no descent direction in the function space. Negative eigenvalues imply that there is a descent direction. To carry out this calculation the integrals of the Coulomb potential required in (106) are obtained by solving the Poisson equation as in (83), and performing the numerical integrals. The calculated eigenvalues are shown in Table 1.

References

- [1] Finite element basis functions. <http://hplgit.github.io>.
- [2] Hypr library. <https://computation.llnl.gov/projects/hypr-scalable-linear-solvers-multigrid-methods>.
- [3] Arnaud Anantharaman and Eric Cancès. Existence of minimizers for Kohn–Sham models in quantum chemistry. *Annales de l'Institut Henri Poincaré (C) Non Linear Analysis*, 26(6):2425–2455, 2009.
- [4] Edoardo Aprà, Eric J. Bylaska, Wibe A. De Jong, Niranjana Govind, Karol Kowalski, Tjerk P. Straatsma, Marat Valiev, Hubertus J.J. van Dam, Yuri Alexeev, James Anchell, and et al. NWChem: Past, present, and future. *The Journal of Chemical Physics*, 152(18):184102, 2020.
- [5] Owe Axelsson and V. Alan Barker. *Finite Element Solution of Boundary Value Problems: Theory and Computation*. SIAM, 2001.

- [6] Randolph E. Bank and Todd Dupont. An optimal order process for solving finite element equations. *Mathematics of Computation*, 36(153):35–51, 1981.
- [7] Giuseppe M. J. Barca, Andrew T. B. Gilbert, and Peter M. W. Gill. Hartree-Fock description of excited states of H₂. *The Journal of Chemical Physics*, 141(11):111104, 2014.
- [8] Rafael Benguria, Haïm Brézis, and Elliott H. Lieb. The Thomas-Fermi-von Weizsäcker theory of atoms and molecules. *Communications in Mathematical Physics*, 79(2):167–180, 1981.
- [9] Dietrich Braess. *Finite elements: theory, fast solvers and applications in solid mechanics, second edition*. Cambridge University Press, 2001.
- [10] James H. Bramble. *Multigrid methods*, volume 294. CRC Press, 1993.
- [11] James H. Bramble and Joseph E. Pasciak. New convergence estimates for multigrid algorithms. *Mathematics of Computation*, 49(180):311–329, 1987.
- [12] Achi Brandt. Algebraic multigrid theory: The symmetric case. *Applied Mathematics and Computation*, 19(1):23–56, 1986.
- [13] Achi Brandt, Steve McCormick, and John Ruge. Algebraic multigrid (amg) for sparse matrix equations. *Sparsity and its Applications*, page 257, 1985.
- [14] Susanne C. Brenner and L. Ridgway Scott. *The mathematical theory of finite element methods*, volume 15. Springer, 2008.
- [15] William L. Briggs, Van Emden Henson, and Stephen F. McCormick. *A multigrid tutorial: second edition*. SIAM, 2000.
- [16] Eric J. Bylaska, Michael Holst, and John H. Weare. Adaptive finite element method for solving the exact kohn-sham equation of density functional theory. *Journal of Chemical Theory and Computation*, 5(4):937–948, 2009.
- [17] Eric J. Bylaska, Scott R. Kohn, Scott B. Baden, Alan Edelman, Ryoichi Kawai, M. Elizabeth G. Ong, and John H. Weare. Scalable parallel numerical methods and software tools for material design. *Proceedings of the Seventh SIAM Conference on Parallel Processing for Scientific Computing*, pages 219–224, 1995.
- [18] Ying Chen, Eric Bylaska, and John Weare. First principles estimation of geochemically important transition metal oxide properties. In James D. Kubicki, editor, *Molecular Modeling of Geochemical Reactions*, chapter 4. Wiley, 2016.
- [19] Aron J. Cohen, Paula Mori-Sánchez, and Weitao Yang. Insights into current limitations of density functional theory. *Science*, 321:792 – 794, 2008.
- [20] Aron J. Cohen, Paula Mori-Sánchez, and Weitao Yang. Challenges for density functional theory. *Chemical Reviews*, 112:289–320, 2012.
- [21] Claude Cohen-Tannoudji, Bernard Diu, and Frank Laloe. *Quantum Mechanics, Volume 1*. Wiley, 1991.
- [22] Paul A. Cox. *Transition Metal Oxides*. Clearendon Press, Oxford, 1992.

- [23] Todd Dupont, Johan Hoffman, Claus Johnson, Robert C. Kirby, Mats G. Larson, Anders Logg, and L. Ridgway Scott. *The FEniCS project*. Chalmers Finite Element Centre, Chalmers University of Technology, 2003.
- [24] James B. Foresman and Aeleen Frisch. *Exploring Chemistry with Electronic Structure Methods*. Gaussian, 1996.
- [25] Rupert L. Frank, Elliott H. Lieb, Robert Seiringer, and Lawrence E. Thomas. Bipolaron and n-polaron binding energies. *Physical Review Letters*, 104(21):210402, 2010.
- [26] Rupert L. Frank, Elliott H. Lieb, Robert Seiringer, and Lawrence E. Thomas. Stability and absence of binding for multi-polaron systems. *Publications mathématiques de l’IHÉS*, 113(1):39–67, 2011.
- [27] Gene H. Golub. *Matrix Computations*. Johns Hopkins Press, 1996.
- [28] David Gontier. Existence of minimizers for Kohn–Sham within the local spin density approximation. *Nonlinearity*, 28(1):57, 2015.
- [29] David Gontier, Christian Hainzl, and Mathieu Lewin. Lower bound on the Hartree-Fock energy of the electron gas. *arXiv preprint arXiv:1811.12461*, 2018.
- [30] David Gontier and Mathieu Lewin. Spin symmetry breaking in the translation-invariant Hartree-Fock uniform electron gas. *arXiv preprint arXiv:1812.07679*, 2018.
- [31] Marcel Griesemer and Fabian Hantsch. Unique solutions to Hartree–Fock equations for closed shell atoms. *Arch. Rational Mech. Anal.*, 203(3):883–900, 2012.
- [32] Wolfgang Hackbusch. *Multi-grid methods and applications*, volume 4. Springer-Verlag Berlin, 1985.
- [33] Robert J. Harrison, George I. Fann, Takeshi Yanai, Zhengting Gan, and Gregory Beylkin. Multiresolution quantum chemistry: Basic theory and initial applications. *The Journal of Chemical Physics*, 121(23):11587–11598, 2004.
- [34] Warren J. Hehre, Robert F. Stewart, and John A. Pople. self-consistent molecular-orbital methods. i. use of gaussian expansions of slater-type atomic orbitals. *The Journal of Chemical Physics*, 51(6):2657–2664, 1969.
- [35] Houdong Hu. Electronic structure models: Solution theory, linear scaling methods, and stability analysis. *UCSD Ph.D. Thesis*, 2014.
- [36] Ricky A. Kendall, Edoardo Aprà, David E. Bernholdt, Eric J. Bylaska, Michel Dupuis, George I. Fann, Robert J. Harrison, Jialin Ju, Jeffrey A. Nichols, Jarek Nieplocha, et al. High performance computational chemistry: An overview of nwchem a distributed parallel application. *Computer Physics Communications*, 128(1):260–283, 2000.
- [37] Eduard Kirr, Panayotis G. Kevrekidis, and Dmitry E. Pelinovsky. Symmetry-breaking bifurcation in the nonlinear Schrödinger equation with symmetric potentials. *Communications in Mathematical Physics*, 308(3):795–844, 2011.
- [38] Scott R. Kohn, John H. Weare, M. Elizabeth G. Ong, and Scott B. Baden. Parallel adaptive mesh refinement for electronic structure calculations. *Proceedings of the Eighth SIAM Conference on Parallel Processing for Scientific Computing*, 1997.

- [39] Claude Le Bris. Some results on the Thomas-Fermi-Dirac-von Weizsäcker model. *Differential and Integral Equations*, 6(2):337–353, 1993.
- [40] Enno Lenzmann. Uniqueness of ground states for pseudorelativistic Hartree equations. *Analysis & PDE*, 2(1):1–27, 2009.
- [41] Elliott H Lieb. Thomas-Fermi and related theories of atoms and molecules. *Reviews of Modern Physics*, 53(4):603, 1981.
- [42] Elliott H. Lieb and Michael Loss. *Analysis*. American Mathematical Society, 2nd edition, 2001.
- [43] Elliott H Lieb and Barry Simon. The Hartree-Fock theory for Coulomb systems. *Communications in Mathematical Physics*, 53(3):185–194, 1977.
- [44] Pierre-Louis Lions. Solutions of Hartree-Fock equations for Coulomb systems. *Communications in Mathematical Physics*, 109(1):33–97, 1987.
- [45] Anders Logg, Kent-Andre Mardel, and Garth N. Wells, editors. *Automated Solution of Differential Equations by the Finite Element method: The FEniCS Book*. Springer, 2012.
- [46] Anders Logg and Garth N. Wells. Dolfin: Automated finite element computing. *ACM Transactions on Mathematical Software (TOMS)*, 37(issue 2, article 20), 2010.
- [47] Stephen F. McCormick. *Multigrid methods*, volume 3. SIAM, 1987.
- [48] G. L. Oliver and J. P. Perdew. Spin-density gradient expansion for kinetic energy. *Physical Review A*, 20(2):397–403, 1979.
- [49] Robert G. Parr. *Quantum Theory of Molecular Electronic Structure*. W. A. Benjamin, 1972.
- [50] Robert G. Parr and Weitao Yang. *Density-Functional Theory of Atoms and Molecules*. Oxford Science Publications, 1989.
- [51] Haowei Peng and John P. Perdew. Synergy of van der waals and self-interaction corrections in transition metal monoxides. *Physical Review B*, 96:100101 1–5, 2017.
- [52] Zachary D. Pozun and Graeme Henkelman. Hybrid density functional theory band structure engineering in hematite. *The Journal of Chemical Physics*, 134:224706–1–9, 2011.
- [53] Michael Reed and Barry Simon. *Analysis of Operators, Vol. IV of Methods of Modern Mathematical Physics*. New York, Academic Press, 1978.
- [54] Julien Ricaud. *Symétrie et brisure de symétrie pour certains problèmes non linéaires*. PhD thesis, Université de Cergy Pontoise, 2017.
- [55] Julien Ricaud. Symmetry breaking in the periodic Thomas–Fermi–Dirac–von Weizsäcker model. *Annales Henri Poincaré*, 19(10):3129–3177, 2018.
- [56] Georg Rollmann, Alexander Rohrbach, Peter Entel, and Jürgen Hafner. First-principle calculations of the structure and magnetic properties of hematite. *Physical Review B*, 69:165107 1–12, 2004.
- [57] David Ruiz. On the Schrödinger–Poisson–Slater system: behavior of minimizers, radial and nonradial cases. *Archive for Rational Mechanics and Analysis*, 198(1):349–368, 2010.

- [58] Mary Beth Ruskai and Frank H Stillinger. Binding limit in the Hartree approximation. *Journal of Mathematical Physics*, 25(6):2099–2103, 1984.
- [59] Yousef Saad and Martin H. Schultz. Gmres: A generalized minimal residual algorithm for solving nonsymmetric linear systems. *SIAM J. Sci. Stat. Comput.*, 7(3):856–869, 1986.
- [60] Catherine Sulem and Pierre-Louis Sulem. *The nonlinear Schrödinger equation: self-focusing and wave collapse*, volume 139. Springer Science & Business Media, 1999.
- [61] Attila Szabo and Neil S. Ostlund. *Modern Quantum Chemistry*. Dover Publications, 1989.
- [62] Osamu Tatebe. The multigrid preconditioned conjugate gradient method. *NASA. Langley Research Center, The Sixth Copper Mountain Conference on Multigrid Methods, Part 2*, 1993.
- [63] Marat Valiev, Eric J. Bylaska, Niranjana Govind, Karol Kowalski, Tjerk P. Straatsma, Hubertus J.J. Van Dam, Dunyou Wang, Jarek Nieplocha, Edoardo Aprà, Theresa L. Windus, and et al. Nwchem: a comprehensive and scalable open-source solution for large scale molecular simulations. *Computer Physics Communications*, 181(9):1477–1489, 2010.
- [64] Henson Van Emden and Ulrike Meir Yang. Boomer amg: A parallel algebraic multigrid solver and preconditioner. *Applied Numerical Mathematics*, 41:155–177, 2002.
- [65] Michael I Weinstein. Lyapunov stability of ground states of nonlinear dispersive evolution equations. *Communications on Pure and Applied Mathematics*, 39(1):51–67, 1986.